EQUILIBRIUM CHARGE DISTRIBUTIONS OF HEAVY IONS FROM 1 MeV TO 48 MeV

by 7214

STEVE A. SAVOY
B.S., University of Southwestern Louisiana, 1969

A MASTER'S THESIS

submitted in partial fulfillment of the

requirements for the degree

MASTER OF SCIENCE

Department of Physics

KANSAS STATE UNIVERSITY
Manhattan, Kansas
1971

Approved by:

James R. Macdonald
Major Professor

THIS BOOK WAS BOUND WITHOUT PAGE ii.

THIS IS AS RECEIVED FROM CUSTOMER.

ILLEGIBLE

THE FOLLOWING DOCUMENT (S) IS ILLEGIBLE DUE TO THE PRINTING ON THE ORIGINAL BEING CUT OFF

ILLEGIBLE

List of Tables

List of Figures

I. INTRODUCTION

If an atom traverses matter it will eventually undergo a collision. The Collision between two atoms can result in a number of phenomena and is generally classified as elastic or inelastic depending on the manner in which energy is transferred. Momenum and energy are transferred from on atom to the translatory motion of the other atom as a whole, and also energy can be transferred to the individual electrons of the other atom. This may result in excitation to higher atomic energy levels, ionization or exchange of electrons between the atoms and characterizes an inelastic encounter. If the energy transferred to the individual electrons is much less than to the translational motion of the whole atom then the collision is said to be elastic.

A. Scattering Cross Section

If some quantitative information about a collision is to be gained, then a model must be used to describe the collision to some degree of approximation. Inelastic effects will be neglected for the moment because electrons in a single collision withe an ion can receive only a small amount of momentum in comparison to a heavy atom. Assuming a simple collisional system in which two charged particles collide and there is a coulombic force between them, then the well known Rutherford scattering formula can be obtained. Following the formulation of Goldstein (1), the differential scattering cross section is given by

$$\sigma(\theta) = - \frac{s}{\sin \theta} \frac{ds}{d\theta} \qquad (1)$$

Fig. 1. Geometry of scattering in the laboratory system.

THIS BOOK CONTAINS NUMEROUS PAGES WITH DIAGRAMS THAT ARE CROOKED COMPARED TO THE REST OF THE INFORMATION ON THE PAGE.

THIS IS AS RECEIVED FROM CUSTOMER.

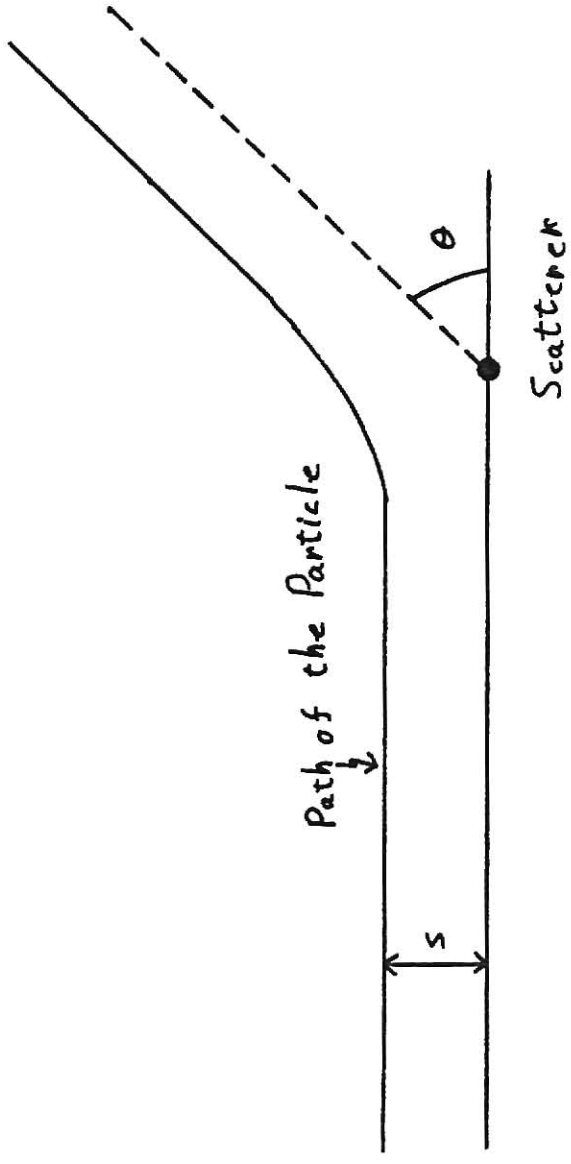

Fig. 1.

where s is the impact parameter and θ is the scattering angle in the laboratory system (Fig. 1). The impact parameter can be written in terms of E and θ, where E is the energy of the scattered particle, so that

$$s = \frac{ZZ'e^2}{2E} \cot(\theta/2) \tag{2}$$

where Z and Z' are the atomic numbers of the particles and e is the electronic charge. By substituting eq. 2 into eq. 1 the differential scattering cross section for fully stripped atomic nuclei is obtained in the form

$$\sigma(\theta) = \frac{1}{4} \left(\frac{ZZ'e^2}{2E}\right)^2 \frac{1}{\sin^4(\theta/2)} . \tag{3}$$

In an actual collisional system the atoms and ions involved will be surrounded by electrons. The electrons will have a screening effect on the pure coulombic potential of the nucleus. Lindhard (2) had written a general form of a screened coulombic potential

$$V(R) = \frac{ZZ'e^2}{R} u \tag{4}$$

where R is the separation between the two atoms and u is the screening function. u is a function of Z, Z' and R only since velocity dependence of the potential is excluded by excluding inelastic effects (2). The function u can be approximated using a Thomas-Fermi potential so that u is a function of R and a,

where a is a characteristic screening length (2). Because of the nature of the Thomas-Fermi approximation no shell effects are evident and only a charge distribution around the ion is considered.

Bohr (3) and Everhart et. al. (4) have used an exponential form for u given as

$$V(\vec{R}) = \frac{ZZ'e^2}{R} \exp(-R/a) \qquad (5)$$

so that $u(R/a) = \exp(-R/a)$. Other forms for u have been used to obtain better representations of the screening effect but Bohr's form provides a good estimate even though it is known qualitatively to fall off too rapidly (2). Using the exponential form the characteristics of a collision can be determined by the relation of the screening length a and the distance of closest approach b, which can be written as

$$b = \frac{2ZZ'e^2}{m_o v^2} \qquad (6)$$

where m_o is the reduced mass of the system and v is the relative velocity. If $b \ll a$ then the effect of screening in the interaction potential will be neglible. The resultant scattering can be described by the Rutherford formula since the ion will see an almost pure coulomb potential. If $b \gtrsim a$ the screening will be significant. The scattering cross section as a function of E, for a certain angle, is plotted in Fig. 2. In region I, $b \gtrsim a$ and a screened field must be used in calculating the scattering whereas in region II, $b \ll a$ and the Rutherford formulation can be applied. If $b \gtrsim a$ then it is known that the exponential screening cuts off the potential too rapidly.

Fig. 2. Differential scattering cross section, at a certain angle, against the energy (2).

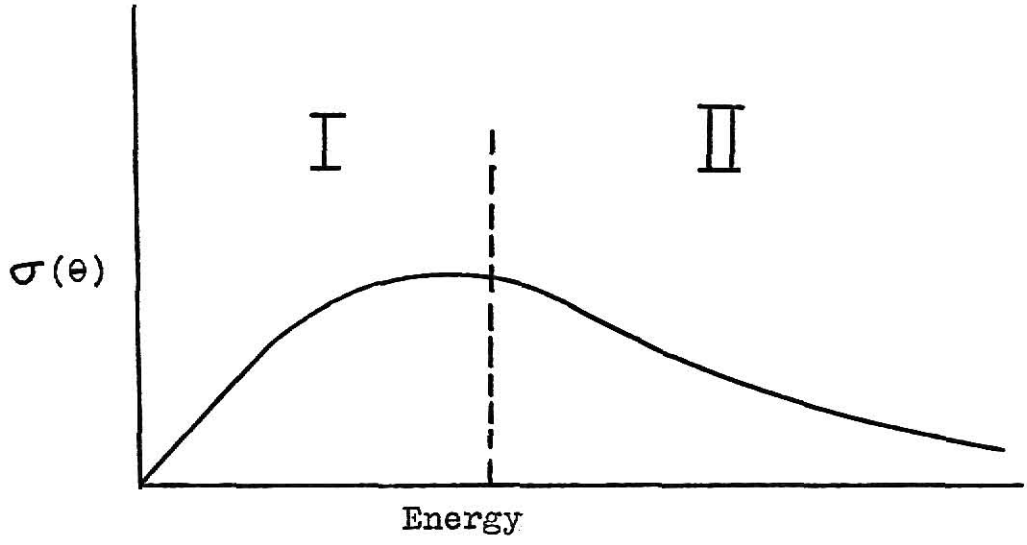

Fig. 2

B. Criterion for the Use of Orbital Pictures

Quantum effects must be considered if the deBroglie wavelength of the ion is of the same order of magnitude as the system dimensions. Using uncertainties due to diffraction effects Bohr (3) has determined a criterion for the applicability of classical orbital pictures in a collisional system. If an ion beam is restricted by a small enough aperature diffraction effects will appear. Given an aperature of diameter d, the divergence of the beam is

$$\delta\varphi = \frac{\lambda\!\!\!^{-}}{d} \tag{7}$$

where φ is the divergence angle and $\lambda\!\!\!^{-} = \hbar/mv$ is the deBroglie wavelength. From the Rutherford scattering formulation

$$\tan\frac{\theta}{2} = \frac{b}{2s} \tag{8}$$

where θ is the deflection angle in the center of mass system. For small deflections

$$\tan\frac{\theta}{2} \approx \frac{\theta}{2} \tag{9}$$

then,

$$\theta \approx \frac{b}{s} . \tag{10}$$

The aperature restricts the accuracy to which the impact parameter may be determined, thereby causing an uncertainty in the

deflection angle. This can be estimated by differentiating equation (10) to obtain

$$\delta\theta = \frac{b}{s^2}\,\delta s. \tag{11}$$

If

$$\delta s = \frac{d}{2} \tag{12}$$

then

$$\delta\theta = \frac{d}{2b}\,\theta^2 . \tag{13}$$

The error inherent in θ can now be written as

$$\Delta\theta = \left[(\delta\varphi)^2 + (\delta\theta)^2\right]^{1/2} . \tag{14}$$

By substituting for $\delta\varphi$ and $\delta\theta$ one obtains

$$\Delta\theta = \sqrt{\frac{\lambda}{b}}\;\theta\left[n + 1/2n\right]^{1/2} \tag{15}$$

where

$$n = \frac{\lambda b}{d^2\theta^2} . \tag{16}$$

By substituting equation (10) for θ then

$$n = \frac{\lambda s^2}{d^2 b} . \tag{17}$$

In order that a classical picture be valid to some degree of accuracy then one can demand that

$$\frac{\lambda}{b} \leq 1. \tag{18}$$

where b can here be used to estimate the minimum dimensions of the scattering system. Now n can be written in the inequality

$$n \leq \frac{s^2}{d^2} \tag{19}$$

and with

$$s = \frac{d}{2} \tag{20}$$

this reduces to

$$n \leq 1/4 \tag{21}$$

and

$$\left[n + 1/4n\right]^{1/2} \geq 1. \tag{22}$$

Hence the uncertainty in the scattering angle is given by

$$\Delta\theta \geq \sqrt{\frac{\lambda}{b}}\,\theta. \tag{23}$$

Bohr defined a parameter χ by

$$\chi = b/\lambda\!\!\!^{-} = 2|e^2ZZ'|/\hbar v \qquad (24)$$

and $\chi \gg 1$ is the necessary and sufficient condition for the justification of classical orbital pictures, since this implies a small uncertainty in θ. For $\chi \gtrsim 1$ orbital pictures loose all their physical significance and some quantum scattering approximation such as a Born approximation must be used.

In this paper the collision of heavy ions of atomic number (Z) from 6-17 and energies from 1 MeV to 54 MeV are considered. The incident ions collide with carbon targets so that χ varies from a minimum value of 14 for a carbon-carbon collision at the lowest velocity to 160 for a chlorine-carbon collision at the maximum chlorine velocity. In general the cases dealt with can be treated using classical orbital theory since in all cases is at least one order of magnitude greater than 1.

C. Multiple Collisions

In this paper only small angle collisions will be considered because the heavy ion beam is observed in the forward direction only. Large angle collisions are the result of many small angle deflections. In most cases considered the number of collisions is large, i.e. greater than 200, so that the distribution of the multiply scattered ions is a Gaussian about the zero scattering angle (5).

D. Energy Loss

In a collisional system elastic effects contribute to the scattering of an ion while inelastic effects predominate in the stopping of a high velocity ion, i.e. one with $v > v_o Z^{2/3}$ where v_o is the velocity of an electron in the first Bohr orbit.

THIS BOOK WAS BOUND WITH TWO PAGES NUMBERED 12. THESE PAGES ARE THE SAME.

THIS IS AS RECEIVED FROM CUSTOMER.

At lower velocities $v \lesssim v\, Z^{2/3}$ the energy loss to atomic recoils becomes the dominant stopping component. In dealing with heavy ions at the energies considered, inelastic effects present complicated problems because the ions carry many bound electrons with them when traveling through matter. There is repeated loss and capture of electrons in the many collisions that the ion undergoes. Eventually some balance is reached between the loss and capture processes. These processes can not be treated exactly but will be approximated by a simple model in the following section of this chapter.

In a single collision with a small deflection angle the energy loss due to elastic effects is much less than the energy loss due to inelastic effects. For a free electron at rest the maximum energy transfer in a collision with a heavy ion is given as (5)

$$\Delta E_{max} = 2mv^2 \tag{25}$$

where m is the electronic mass and v is the velocity of the ion. Assuming a velocity of $6(10^8)$cm/sec. (for example, the velocity of chlorine ions at about 8 MeV) the maximum energy transfer is 0.41 keV. This energy can be compared to the energy transferred in the collision of two carbon ions which is (5)

$$\Delta E(s) = \frac{Z^2 Z'^2 e^4}{2Mv^2}\left[\frac{1}{s^2}\right]. \tag{26}$$

If s is assumed to be equal to a_o and v is assumed to be $6(10^8)$ cm/sec. then $\Delta E(a_o) = 0.1eV$. The difference in the energy transfered for the two cases is approximately three orders of magnitude. The elastic scattering events will contribute a neglible

At lower velocities $v \lesssim v_0 Z^{2/3}$ the energy loss to atomic recoils becomes the dominant stopping component. In dealing with heavy ions at the energies considered, inelastic effects present complicated problems because the ions carry many bound electrons with them when traveling through matter. There is repeated loss and capture of electrons in the many collisions that the ion undergoes. Eventually some balance is reached between the loss and capture processes. These processes can not be treated exactly but will be approximated by a simple model in the following section of this chapter.

In a single collision with a small deflection angle the energy loss due to elastic effects is much less than the energy loss due to inelastic effects. For a free electron at rest the maximum energy transfer in a collision with a heavy ion is given as (5)

$$\Delta E_{max} = 2mv^2 \tag{25}$$

where m is the electronic mass and v is the velocity of the ion. Assuming a velocity of $6(10^8)$cm/sec. (for example, the velocity of chlorine ions at about 8 MeV) the maximum energy transfer is 0.41 keV. This energy can be compared to the energy transferred in the collision of two carbon ions which is (5)

$$\Delta E(s) = \frac{Z^2 Z'^2 e^4}{2Mv^2}\left[\frac{1}{s^2}\right]. \tag{26}$$

If s is assumed to be equal to a_0 and v is assumed to be $6(10^8)$ cm/sec. then $\Delta E(a_0) = 0.1$eV. The difference in the energy transfered for the two cases is approximately three orders of magnitude. The elastic scattering events will contribute a neglible

amount to the energy loss as compared to the loss due to electronic collisions at higher energies.

E. Loss and Capture Cross Sections

The process of loss or capture of an electron by an ion traveling through matter can be considered in a first approximation using only momentum and energy transfer arguments. If an electron is to be lost it must gain enough energy to break its binding energy to the ion. The inner shell electrons have large binding energies in comparison to the outer shell ones so that the probability of loss of these is very small. At lower velocities, i.e. slightly greater than v_o, the ions will not be highly ionized but at higher velocities the outer electrons can gain more than the binding energy in a collision and the ion will become more highly ionized. At energies of about 40 MeV most of the heavy ions used in these experiments will be fully stripped of all electrons with binding energies less than several hundred eV.

An estimate of the loss cross section for electrons of a heavy ion has been obtained by Bohr (3). The assumption was made that an electron is lost from an ions if the energy transfered in a collision exceeds the binding energy of the electron. The cross section for energy transfer greater than T to a free electron in a collision is given as

$$\sigma = 2\pi a_o^2 Z_1^{*2} (v_o/v)^2 (mv_o^2/T - mv_o^2/T_{max} \qquad (27)$$

where $T_{max}=2mv^2$ is the maximum energy transfer in the collision, Z_1^* is the effective charge of an atom for removing the electron. Z_1 denotes the atomic number of the atom and Z_2 of the ion.

Using $T = mv_e^2/2$ and the Thomas-Fermi velocity distribution

approximately given by Bohr and Lindhard (6) as

$$dn_e = Z_2^{1/3}(dv_e/v_o) \tag{28}$$

where v_e is the electronic velocity, n_e is the number of electrons and Z_2 is the atomic number of an ion. The cross sections for loss can be obtained by summing eq. 27 over all electrons with velocities less than v_e. The result obtained by Bohr and Lindhard (6) for this is

$$\sigma_l = \pi a_o^2 Z_1^* Z_2^{1/3}(v_o/v_e)^3 \tag{29}$$

as an estimate of the loss cross section. This cross section is only an estimate of the loss cross section. This cross section is only an estimate since the effect of the electron binding is neglected as is the excitation energy which may cause one or more electrons to be ejected in an Auger process resulting from a rearrangement of the electrons of the ion. In some cases the electrons may be in an excited state initially as a result of earlier collisions so that the energy needed for loss will be less.

The process of capture is more complicated since the electron that is to be captured must gain enough momentum so that its energy in the rest mass system of the ion is negative. It is possible that a slow electron could gain enough energy through a collision so that it would be captured but this process is not very probable because it requires a transfer of momentum in a three body interaction as well as the emission of photons to provide binding. The complexity of the problem is very great and the probability is low. It is most likely that the electron

which is captured already has a velocity comparable to the velocity of the ion; for example high velocity ions are likely to capture inner shell electrons of the atoms of the stopping material.

Bohr and Lindhard (6) have treated the capture process by considering the electrostatic forces exerted on the electron both by the atom and the ion. When a highly charged ion approaches an atom, the ionic field may repture the bond between an electron and the atom. The distance at which the release occurs can be estimated by assuming that the force on the electron

from the ion is approximately equal to the binding force when the release takes place. This can be written as

$$\frac{Z_a^* e^2}{R^2} = \frac{mv^2}{a} \qquad (30)$$

where R is the distance between the two systems at the time of release, v and a are the orbital velocity and radius of the electron in the atom.

Bell (7) has given a criterion which relates velocity conditions of the released electron with requirements for capture in the following manner. If the initial kinetic energy of the electron in the rest mass system of the ion is small enough that capture is possible, then a criterion for capture is

$$|\vec{v}_e + \vec{v}| < v_o \qquad (31)$$

where v_o is the minimum speed relative to the ion that an electron at a distance R_o must have in order to escape. The capture radius R_o is related to the velocity of the ion through equation (31) and the following equation:

$$\frac{Z_a^* e^2}{R_o} = mv_o^2/2 \qquad (32)$$

Capture will occur if the release radius R is less than R_o and capture occurs with a cross section of πR^2. This criterion restricts electron capture to electrons with velocities near the velocity of the ion. A free electron will be captured with a neglible probability since in the rest mass system of the ion

it has a large velocity, and since v is large, R_o is small.

In the case of heavy ion electrons Lindhard and Bohr (6) have stated that only electrons with orbital velocities around $\bar{v}/2$ will be captured so that using equations 27 and 28 the capture cross section can be estimated as

$$\sigma_c = \pi a_o^2 Z_2^{*2} Z_1^{1/3} (v_o/v)^3 . \qquad (33)$$

F. Equilibrium

As a heavy ion travels through matter a balance between loss and capture will eventually occur at a given velocity. This balance will continually change since the processes of loss and capture will change the velocity of the ion thereby changing the cross sections for loss and capture.

After an ion travels through matter a number of charge states will emerge. The fraction of ions in each charge state depends on the cross sections for loss or capture into the various states at different energies. A plot of the various charge fractions against the ion energy (Fig. 3) shows the relative number of ions in each charge state at different energies. It can be seen that as the energy and velocity of the ion increases, more and more electrons are lost by the ion and the mean charge of the beam approaches that of a fully stripped atom.

As the ion travels through matter an equilibrium condition will be reached. An equilibrium in the thermodynamic sense is not established, however the terminology used consistently in the literature refers to an equilibrium charge distribution at a given velocity to describe the condition of the beam when capture and loss processes are balanced. Whether or not equilibrium has been reached is determined by two different methods. First, if the emergent distribution is the same when the charge state of the incident ion is changed then equilibrium has been established. Secondly, if the emergent distribution is not

Fig. 3. A plot of charge fractions against the ion energy.

THIS BOOK CONTAINS NUMEROUS PAGES WITH DIAGRAMS THAT ARE CROOKED COMPARED TO THE REST OF THE INFORMATION ON THE PAGE.

THIS IS AS RECEIVED FROM CUSTOMER.

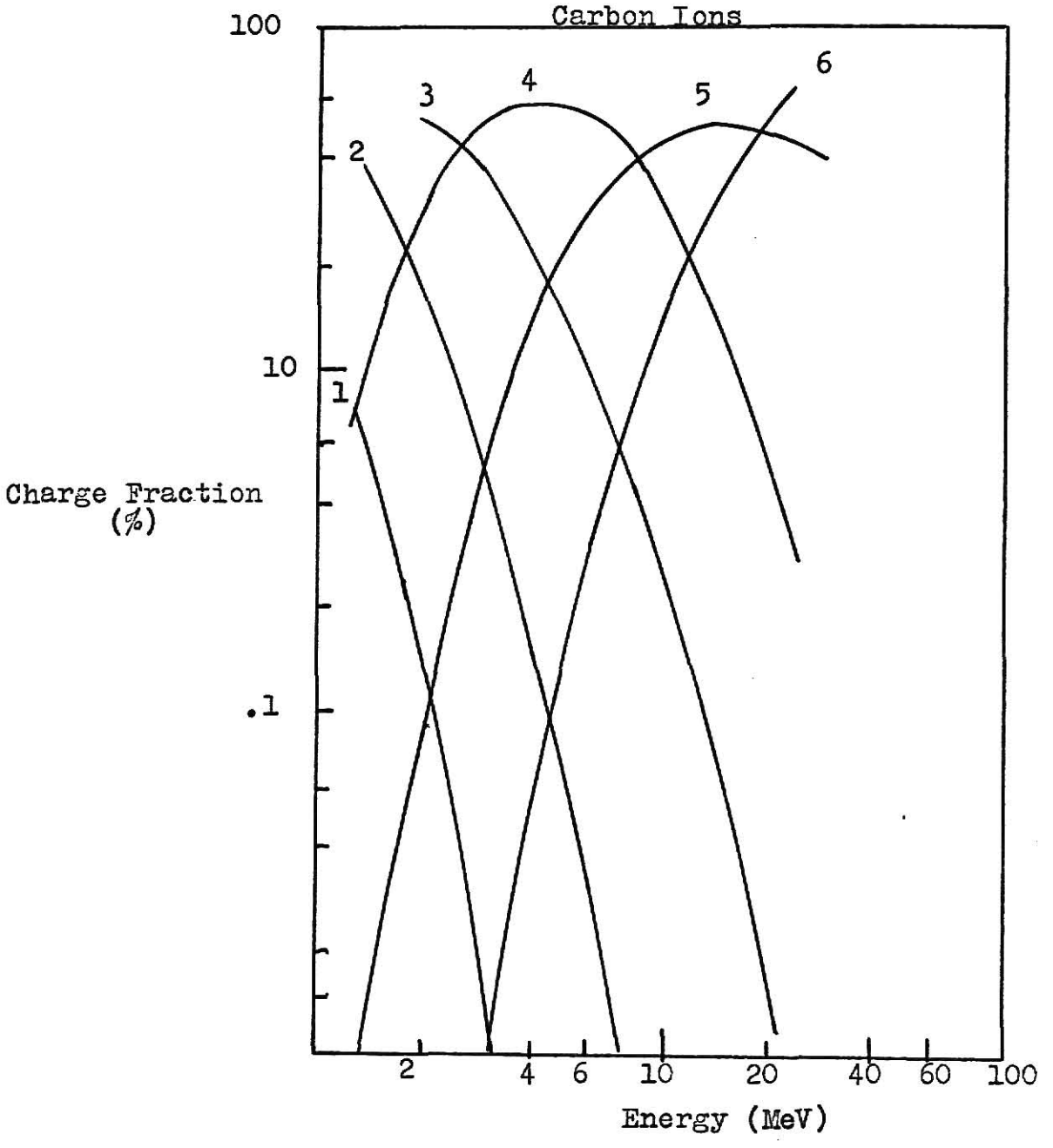
Carbon Ions
100
10
1
.1
Charge Fraction
(%)
1
2
3
4
5
6
2
4
6
10
20
40
60
100
Energy (MeV)

Fig. 3

changed by varying the thickness of the matter through which the ion passes then a balance condition exists in the beam. However, if the thickness is varied enough the cross sections will also begin to change because of the energy dependence and the distributions will change especially in the less dominant charge states. The dominant charge fractions will not vary appreciably since the ratio of the cross sections for these states will not be a rapidly changing function of velocity. The second condition is still a good approximation in determining whether equilibrium has been reached if the thickness is not varied too much.

The rate of change of charge fractions in an ion beam can be expressed in terms of a set of differential equations (8)

$$\frac{d\varphi_k}{dx} = \sum_{j \neq k} \sigma_{jk}\varphi_j - \sigma_{kj}\varphi_k \qquad (34)$$

where φ_k is the fraction of ions in the charge state k, φ_j is the fraction in the charge state j, σ_{jk} is the cross section for charge exchange in which an ion of charge j looses or captures an electron(s) so that its final charge state is k and x is the amount of matter traversed in atoms/cm^2.

If the amount of matter traversed is infinite, then equilibrium is established and from equation (34)

$$\frac{d\varphi_k}{dx} = 0 \qquad (35)$$

If one ignores multiple transfer events (experimentally the cross section is reduced by a factor of 4-8 for each additional

electron transferred) in a single collision then one obtains the following relation between the cross sections and equilibrium charge fractions (8)

$$\frac{F_{i+1}}{F_i} = \frac{\sigma_{i,i+1}}{\sigma_{i+1,i}} \qquad (36)$$

where F_k denotes equilibrium charge fractions.

If there are electrons in states other than the ground state the cross section for charge exchange from each of the excited states will be different. In experiments with gas targets the density can be made low enough that the time between collisions is longer than the lifetime of the excited states; then these states will decay before another collision occurs and the cross sections and equilibrium distributions for the ground state or perhaps several metastable states are determined. As the target density increases the time between collisions decreases, so that in the case of a solid target, many of the electrons are in excited states when the collision occurs and all cross sections measured are complicated averages over those for the states of the ion.

If thin target conditions exist the charge of the incident ion can be varied and the charge fractions which emerge can be measured. By changing the incident charge states at each energy then equation (35) can be solved for all cross sections. These cross sections will all be for charge exchange from the ground state.

In the case of solids only the ratios of cross sections can be determined as the ratio of known equilibrium charge fractions are known. From eq. 29 and 33 an estimate of the velocity dependence of the ratio of capture and loss cross sections can be obtained. The ratio can be written as

$$\frac{\sigma_c}{\sigma_l} = \frac{Z_1^{1/3}}{Z_2^{1/3}} \left(\frac{v_e}{v}\right)^3 \qquad (37)$$

where Z_1 is the number of the stopping material, Z_2 is the atomic number of the ion, v is the velocity of the ion and v_e is the velocity of the electron. If v_e=v then σ_c/σ_l is constant, i.e. a balance between the loss and capture cross sections is reached. It is implied in eq.37 that the velocity dependence of the ratio F_i/F_{i+1} is expected to be as v^{-3} at high velocities.

As an ion travels through matter and is slowed the capture and loss cross sections change so that the mean degree of ionization ($\bar{i}/Z$) will also change. Bohr (18) has stated that an ion traveling through matter retains only those electrons with velocities comparable to the velocity of the ion. If this criterion were to hold rigorously then a plot of the mean ionization against the velocity of the ion would show definite structure indicating the different velocities and ionization potentials of the electrons in each shell. This structure is not observed in an actual case because the mean ionization depends on the number of electrons in the outer shell of the ion, the extent of filling in the shells and the effective charge of the ion core (8). As a better approximation Bohr (3) using a statistical model has found that

$$\bar{i}/Z = 1/Z^{2/3}(v/v_o) \qquad (38)$$

Later a comparison will be made between the mean ionization and charge fraction ratios and the experimental data of this experiment.

II. Experimental Apparatus and Procedure

The heavy ion beams used in the experiment were obtained from the Kansas State University Tandem Van de Graaf accelerator(Fig.4). The energy of the ion was selected by varying the potential of the accelerator terminal and choosing an appropiate charge state of the ion with the desired magnetic rigidity in the energy analyzing magnet. Negatively charged ions are extracted directly from the ion source, accelerated to the positive terminal voltage, stripped of one or several electrons and accelerated again to ground potential. The energy of the ion that emerges from the accelerator is given by $E=(n+1)V + V_s$ where n is the charge of the ion after it is stripped at the terminal, V_s is the potential of the source and E is the energy of the emergent ion at a terminal voltage V.

The ions that emerge have an energy distribution different for each emerging charge state. In order to precisely determine the energy of the ions used in the experiment, the analyzing magnet is used to select the proper magnetic rigidity of a particular charge state and to control the accelerator at the proper terminal voltage. The magnetic field of the analyzing magnet was measured using an NMR fluxmeter that has been calibrated with a known proton resonance. The accuracy of the energy determination was $\pm$ 10 keV.

The ions were then incident upon a carbon foil of thickness from 10-40$\mu g/cm^2$. After traversing the foil an equilibrium condition was obtained and various charge fractions emerged.

The charge distributions of the ions were determined using two different procedures. In the first method, the ions in various charge states that emerged from the foil were directed by the switching magnet into a large Faraday cup (Fig.5) at the 45° deflection port. By scanning the magnet the different charge states were deflected one by one into the Faraday cup which was located within the field of the switching magnet and

Fig. 4. Schematic of Tandem Van de Graaf accelerator.

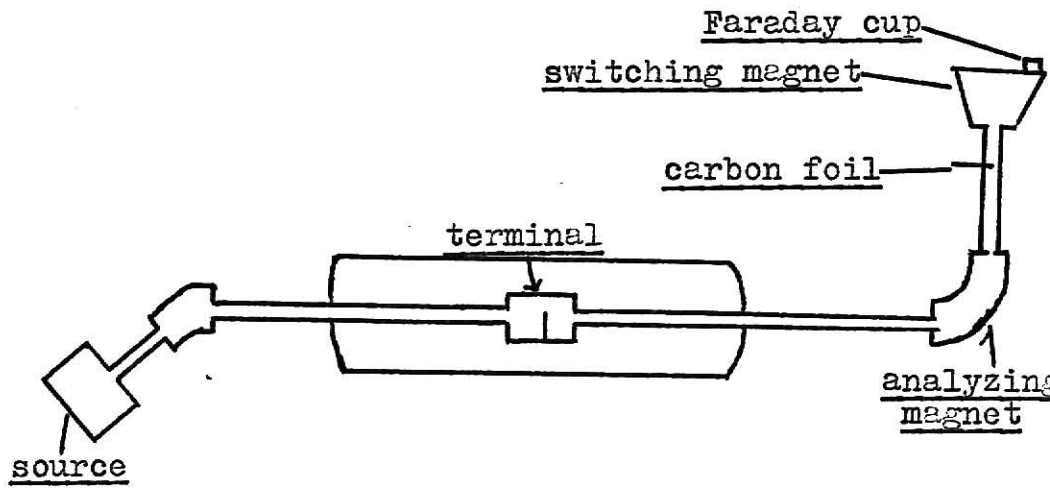
Faraday cup
switching magnet
carbon foil
terminal
analyzing magnet
source

Fig. 4

Fig. 5 Faraday cup. 'A' denotes picoammeter.

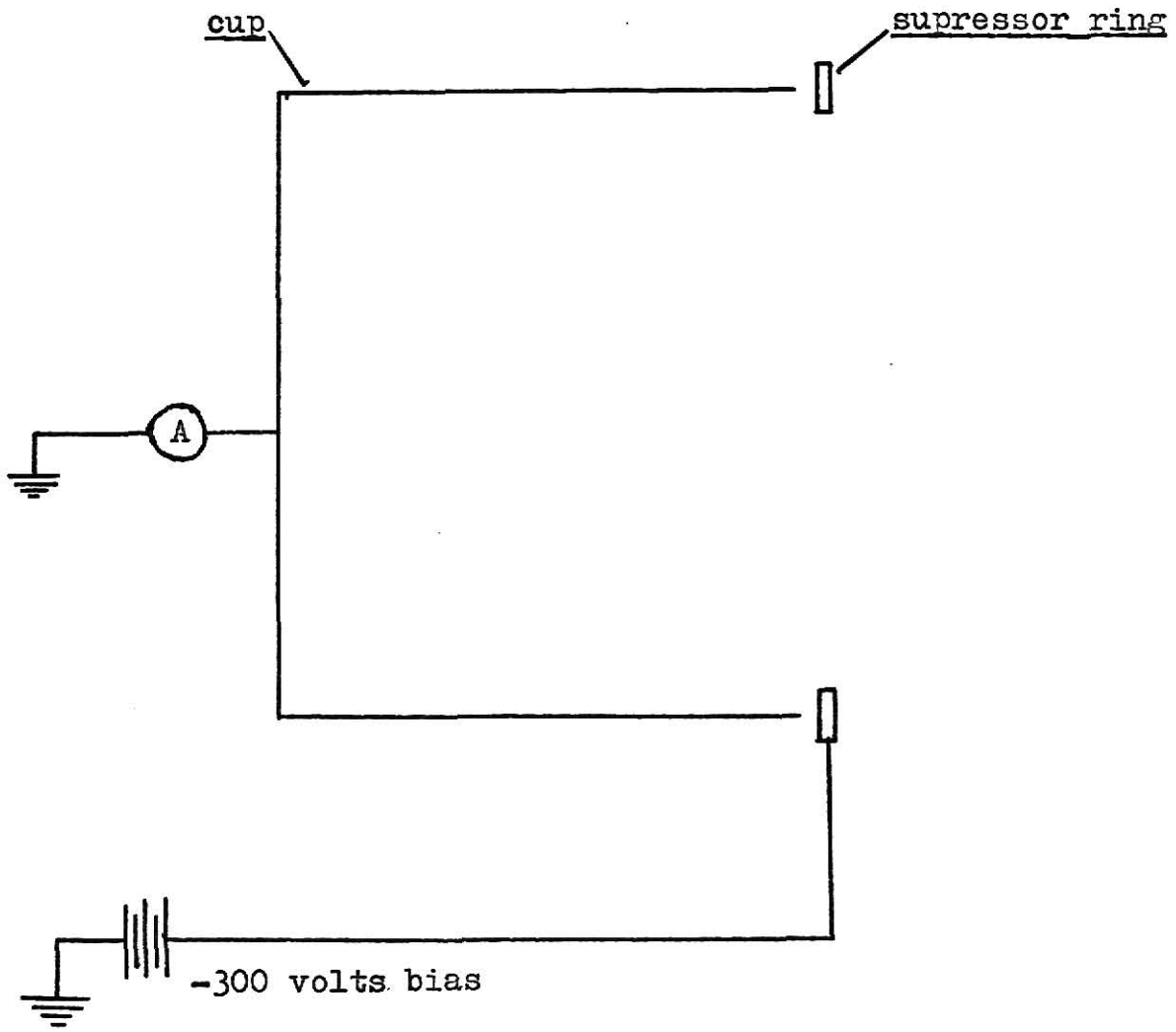

Fig. 5.

was suppressed with a voltage of -300 volts at the entrance. The amount of beam current in each charge state was measured using a Keithly Model 414A picoammeter. From the current measured in each charge state the number of ions per second were determined and the distribution of ions in each charge state was calculated.

In the second method used, (Fig.6) the ions from the analyzing magnet were incident upon the carbon foil and one particular charge state was selected by the switching magnet. The beam then traveled down the beam line and was incident upon another carbon foil. After traversing the foil the beam traveled through a set of aperatures which were 0.5mm, 1mm, 1mm, and 2mm in diameter. The charge states were separated by a magnet and deflected onto a position sensitive detector supplied by Nuclear Diodes Inc. .

The position sensitive detector consists of a silicon surface barrier detector with a resistive layer on the back (Fig.7). When a particle enters the detector electron-hole pairs are produced at a rate of one electron-hole pair for each 3.6 eV of energy deposited in the detector. The electrons travel to ground through the resistance layer and the holes to the biased gold layer. The resistance layer AB (Fig.8) is a resistance across the terminal of the preamplifier. If a particle enters the detector at R then the corresponding position signal of pulse height P(R) arrives at the preamplifier through a resistance equal to X where the total resistance of the layer is X+Y. The energy and the total resistance are constant so that the position pulse can be related to the energy pulse by the equation

$$P(R) = \frac{Y}{X + Y} E \qquad (39)$$

Fig. 6. Experimental setup for position sensitive detector.

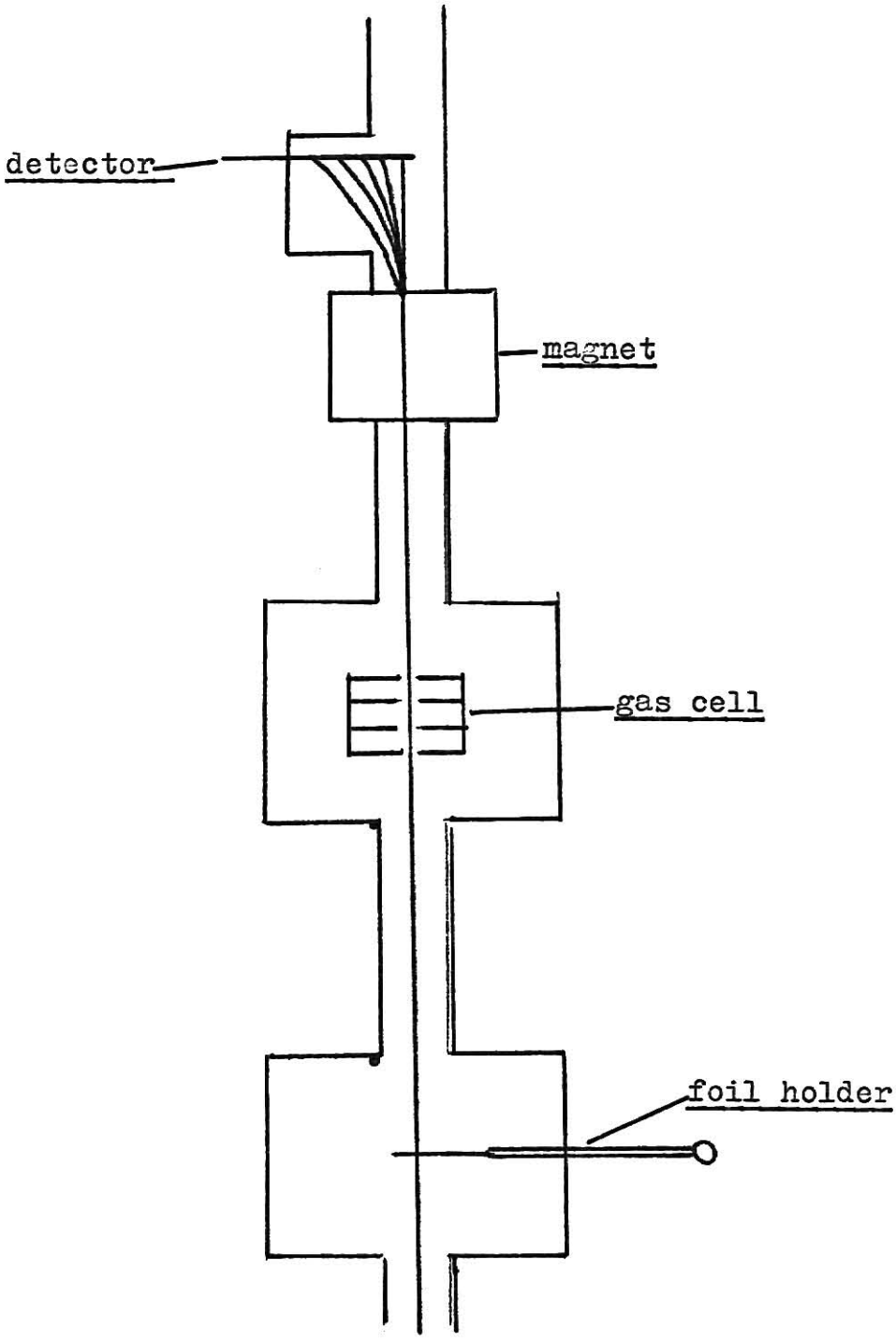

Fig. 6

Fig. 7. Position sensitive detector.

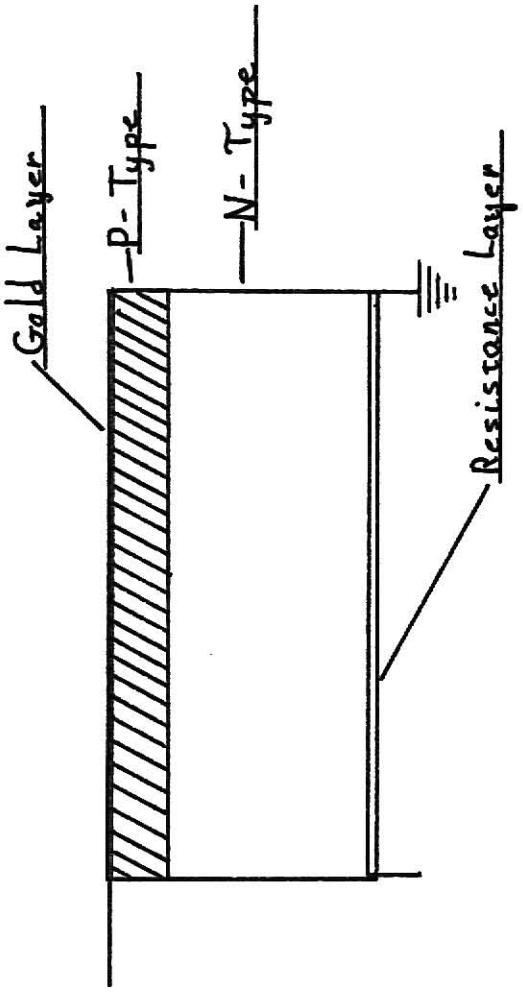

Fig. 7

Fig. 8. Position sensitive detector resistance layer. R is the positon of the particle and the resistance layer is of length AB.

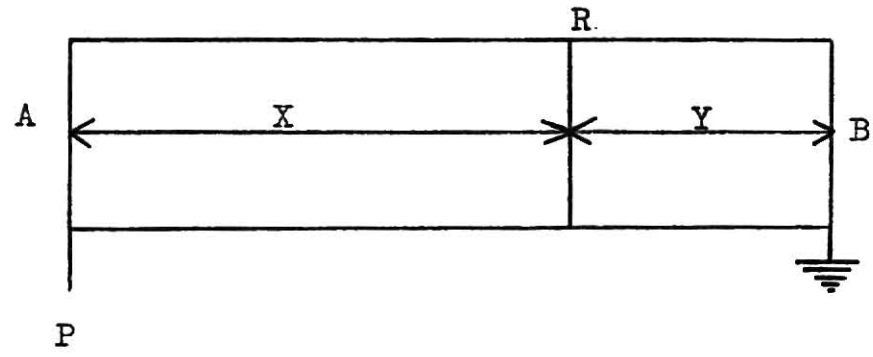

Fig. 8

The position and energy pulses then go to preamplifiers and amplifiers (Fig.9). A single channel analyzer which is set on the energy pulse to select out only the particles of the correcto energy. The pulses that are allowed through the SCA go to a gate and delay generator which generates the gate for the ADC. A pulse divider was used to remove the energy dependence from the position pulse. Since the detector has a different energy signal at different positions the divider improves the resolution of the position spectrum obtained. After the data is accepted by the ADC and analyzed on the TMC analyzer it is then stored on magnetic tape. A computer program was used to obtain a spectrum print-out. The spectra obtained are plots of the number of counts per channel against the channel number corresponding to the position (Fig. 10).

At each energy and incident charge state three position spectra were taken in order to determine accurate charge distributions. In order to identify the charge states a spectrum was taken without a foil so that the position of the incident charge state could be determined. Since the detector position and the deflecting magnetic field were not changed for the data giving an equilibrium distribution emerging from the foil the identification of each charge state could be determined in the second spectrum. Care was taken that the magnetic field was at such a value that the highest charge states were located at approximately the center of the detector. The third spectrum was taken with greater magnetic deflection such that the lowest charge states were on the detector. These two charge distribution spectra were taken so that all the charge states could be detected with accuracy. If a charge state is close to the edge of the detecting surface the number of ions detected may be smaller than the total number for that charge state because some particles may miss the active area of the detector. By taking a spectrum at different magnetic fields an accurate determination of the charge fractions was possible even in the highest charge states.

Fig. 9. Electronics setup.

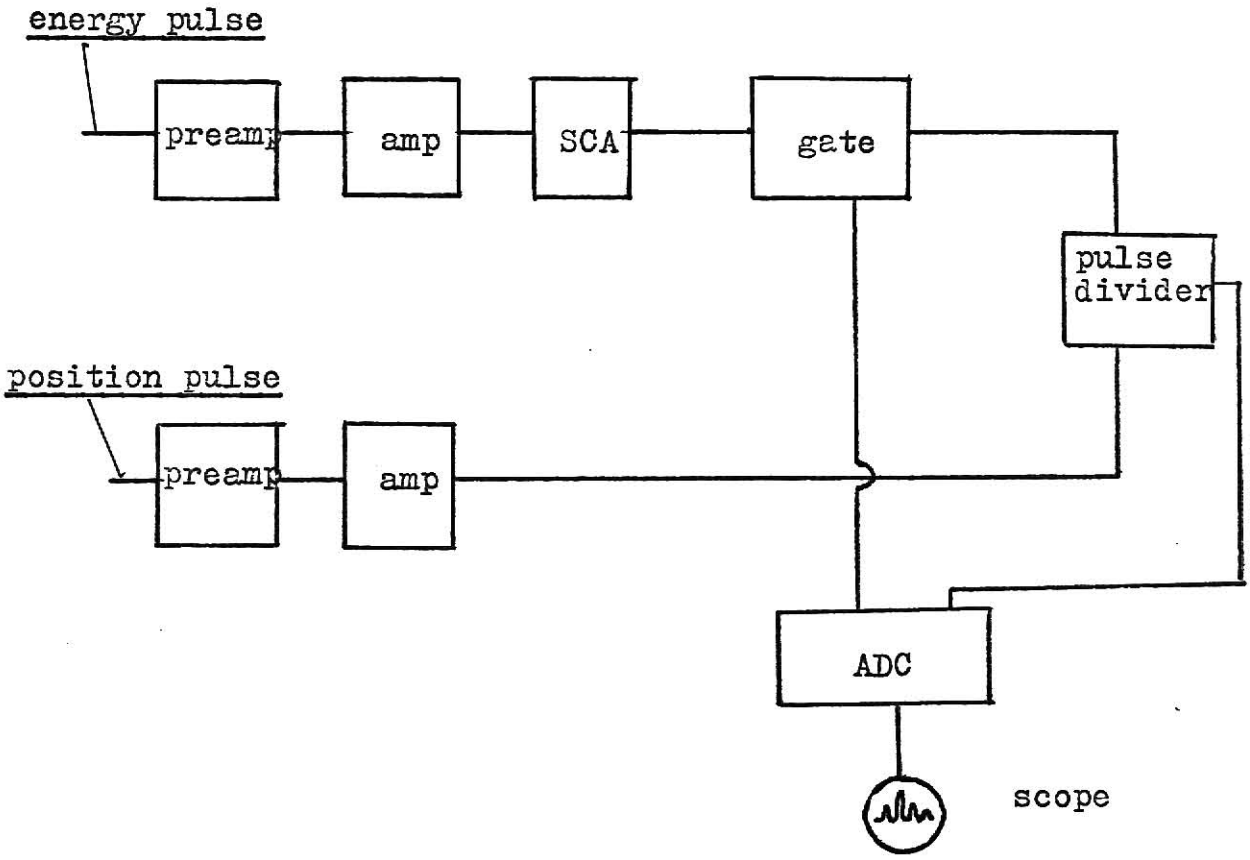
energy pulse
preamp
amp
SCA
gate
pulse divider
position pulse
preamp
amp
ADC
scope

Fig. 9

Fig. 10. Spectra of equilibrium charge distribution.

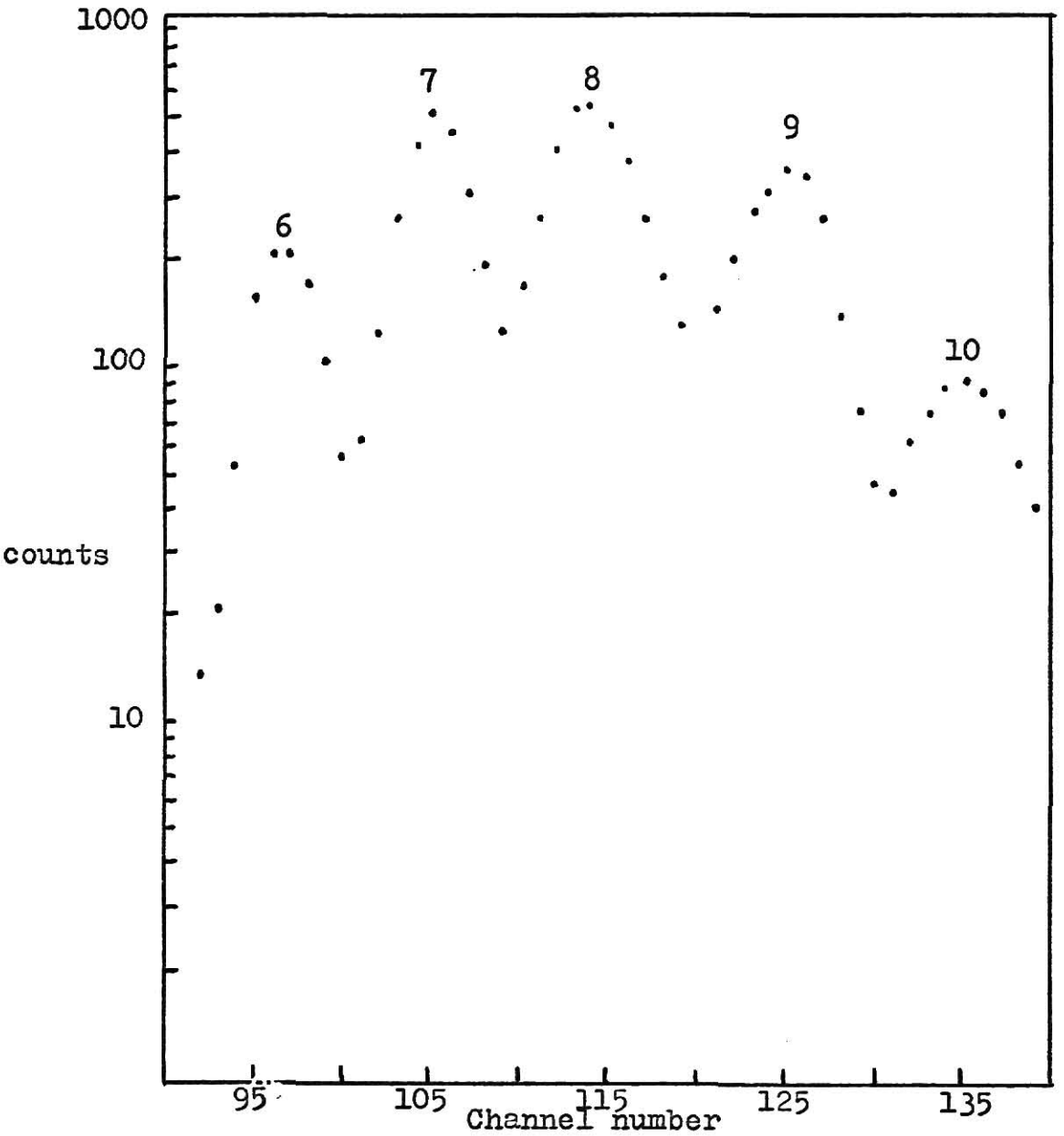

Fig. 10

III. Results

Equilibrium distributions were obtained for carbon, nitrogen, fluorine and chlorine ions from 1 MeV to 48 MeV. Non-equilibrium distributions were measured for 51 MeV and 54 MeV chlorine ions in carbon stripping foils. The equilibrium distributions are shown in Figs. 11, 12, 13, and 14. The non-equilibrium data is given in Table I.

At energies up to and including 48 MeV equilibrium was reached in a 10 $\mu g/cm^2$ foil. From this data less than 10^{18} atoms/cm^2 are required for equilibrium. This effect has been stated only qualitatively in the past.

Previous measurements have been made by Almqvist et. al. (9), Wolke and Snodd (10), F. W. Martin (11) and Preekschat and Vandenbosch (12) in carbon strippers. This data is compared with the present results in Figs. 15, 16 and 17. Because of the complexity of the plots smooth curves have been drawn through the data of this experiment and the individual points represent the work of other authors.

Data of equilibrium distributions in other stripping materials have also been compared with the present measurements in the same manner as above. These points have been measured by Reynolds et. al. (13), Heckman et. al. (14) and Nikolaev et. al. (16). These data are compared to the results of this experiment in Figs. 15, 16 and 17. The data have been obtained in different stripping foils such as Zapon, formvar, nickel, etc. .

Fig. 11. Equilibrium charge distribution of carbon ions.

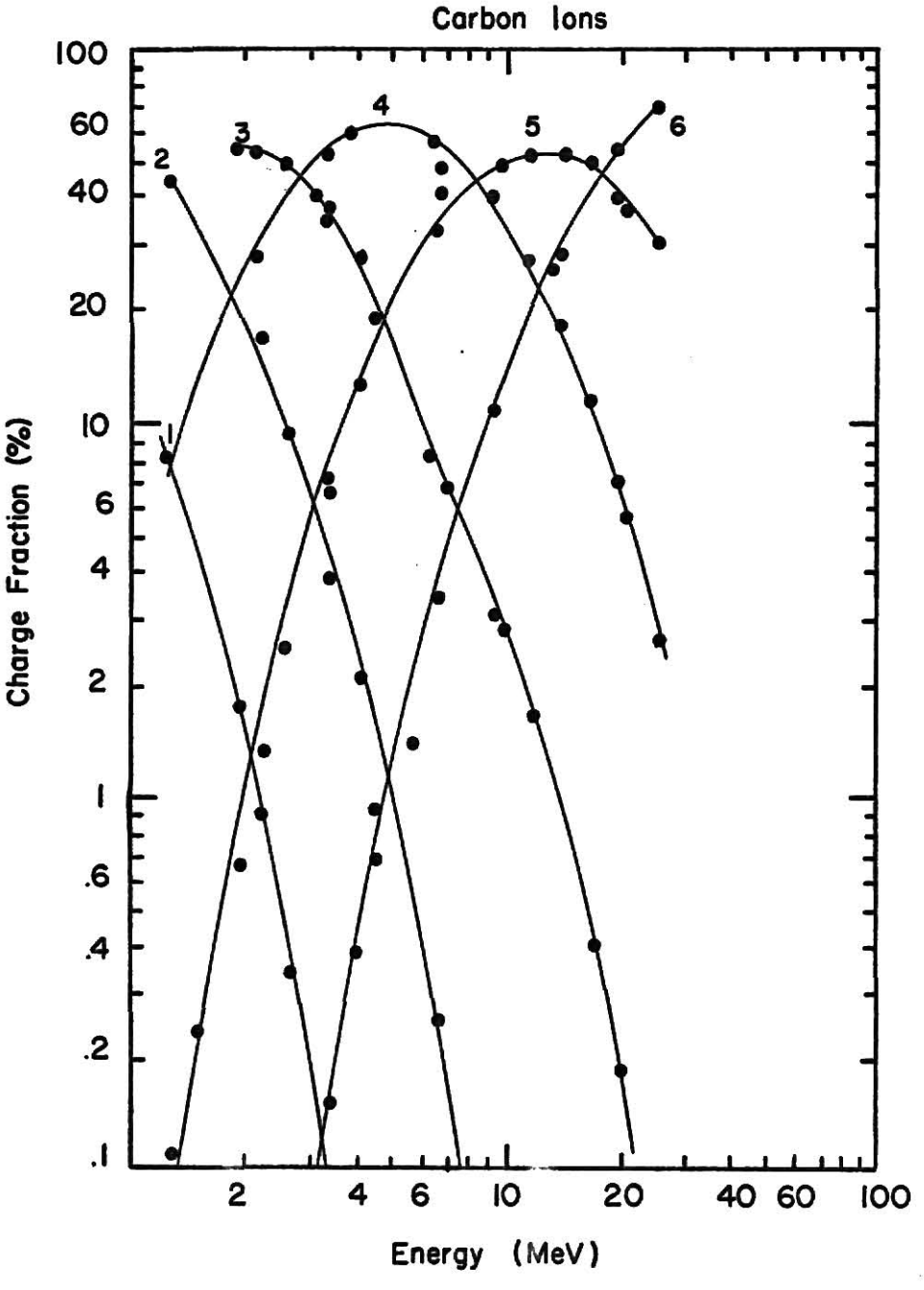
Carbon Ions
Charge Fraction (%)
100
60
40
20
10
6
4
2
1
.6
.4
.2
.1
1
2
3
4
5
6
2
4
6
10
20
40
60
100
Energy (MeV)

Fig. 11

Fig. 12. Equilibrium charge distributions of nitrogen ions.

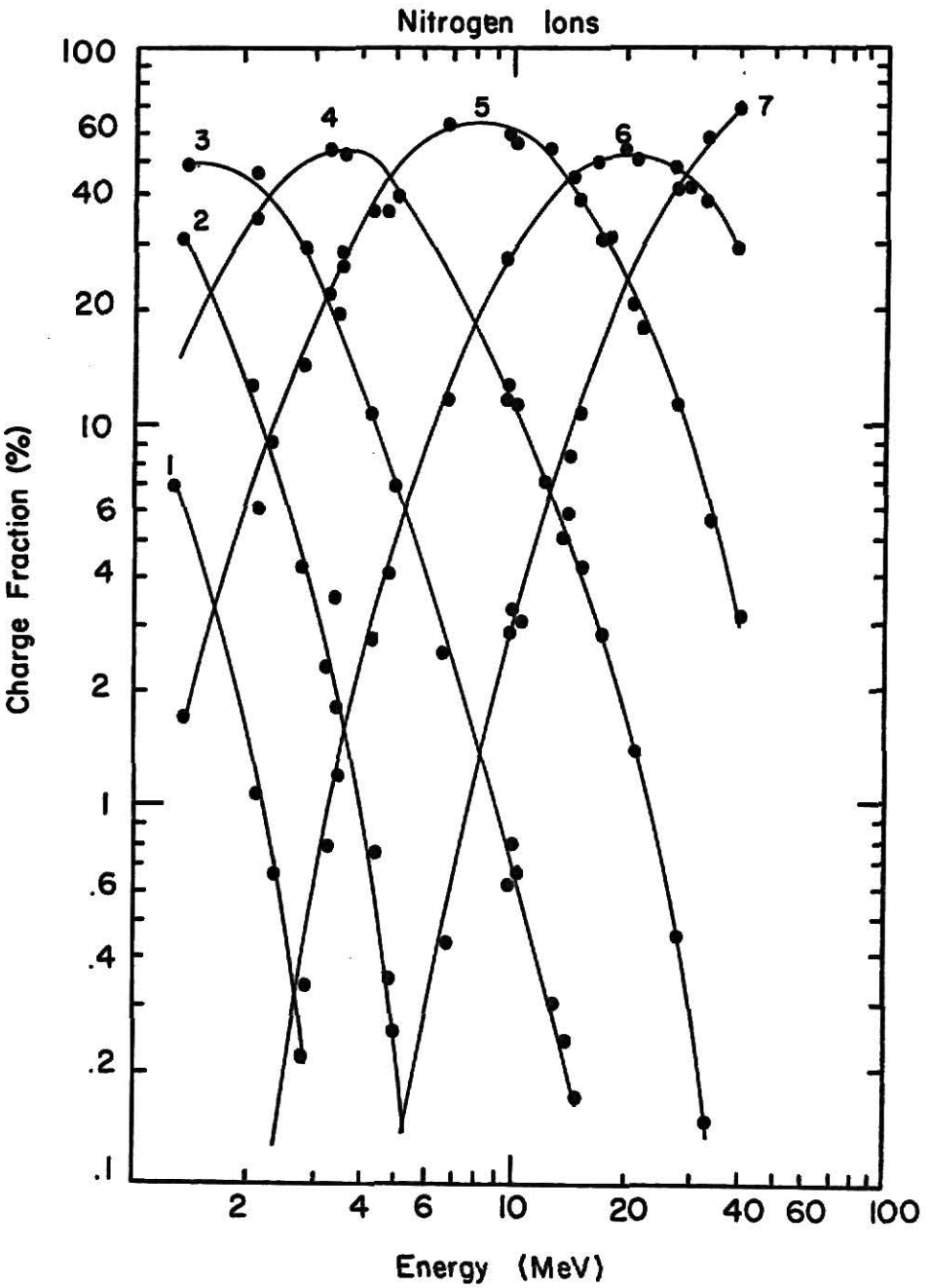
Nitrogen Ions
Charge Fraction (%)
100
60
40
20
10
6
4
2
1
.6
.4
.2
.1
1
2
3
4
5
6
7
2
4
6
10
20
40
60
100
Energy (MeV)

Fig. 12

Fig. 13. Equilibrium charge distributions of fluorine ions.

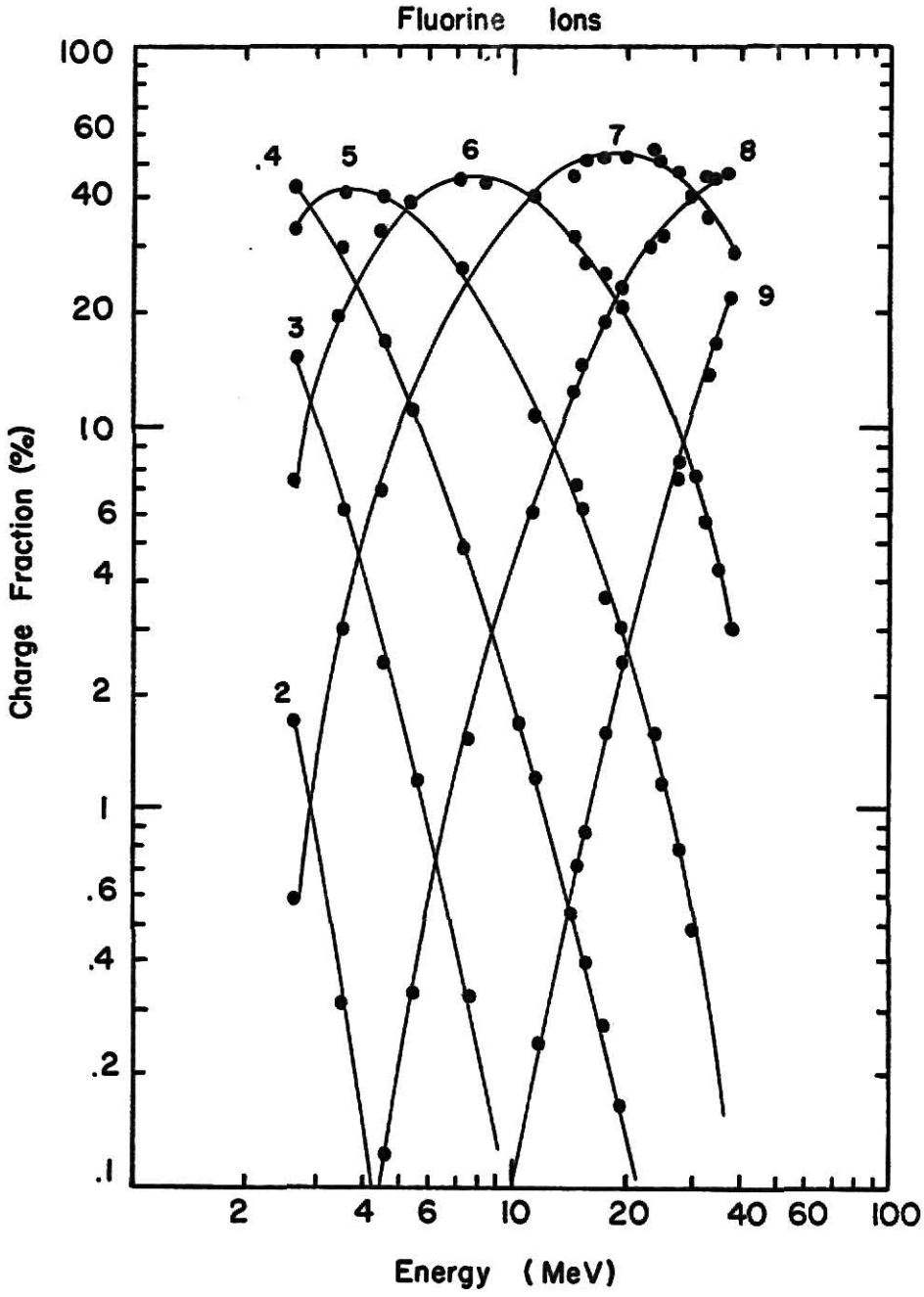
Fluorine Ions
Charge Fraction (%)
100
60
40
20
10
6
4
2
1
.6
.4
.2
.1
2
4
6
10
20
40
60
100
Energy (MeV)
2
3
4
5
6
7
8
9

Fig. 13

Fig. 14. Equilibrium charge distributions of chlorine ions.

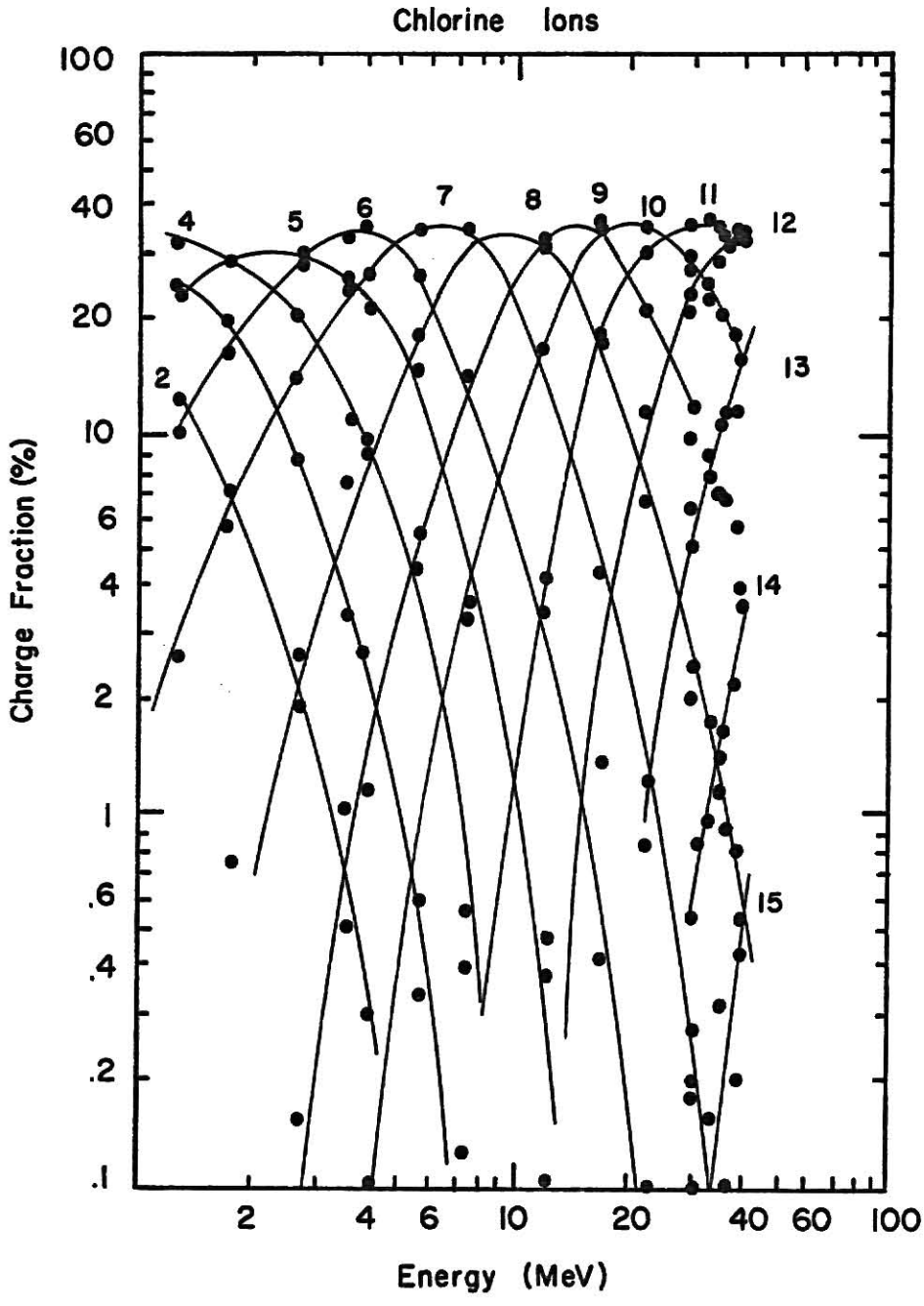
Chlorine Ions
Charge Fraction (%)
100
60
40
20
10
6
4
2
1
.6
.4
.2
.1
2
4
6
10
20
40
60
100
Energy (MeV)
2
4
5
6
7
8
9
10
11
12
13
14
15

Fig. 14

Fig. 15. Comparison of previous carbon data with the carbon data of this experiment.

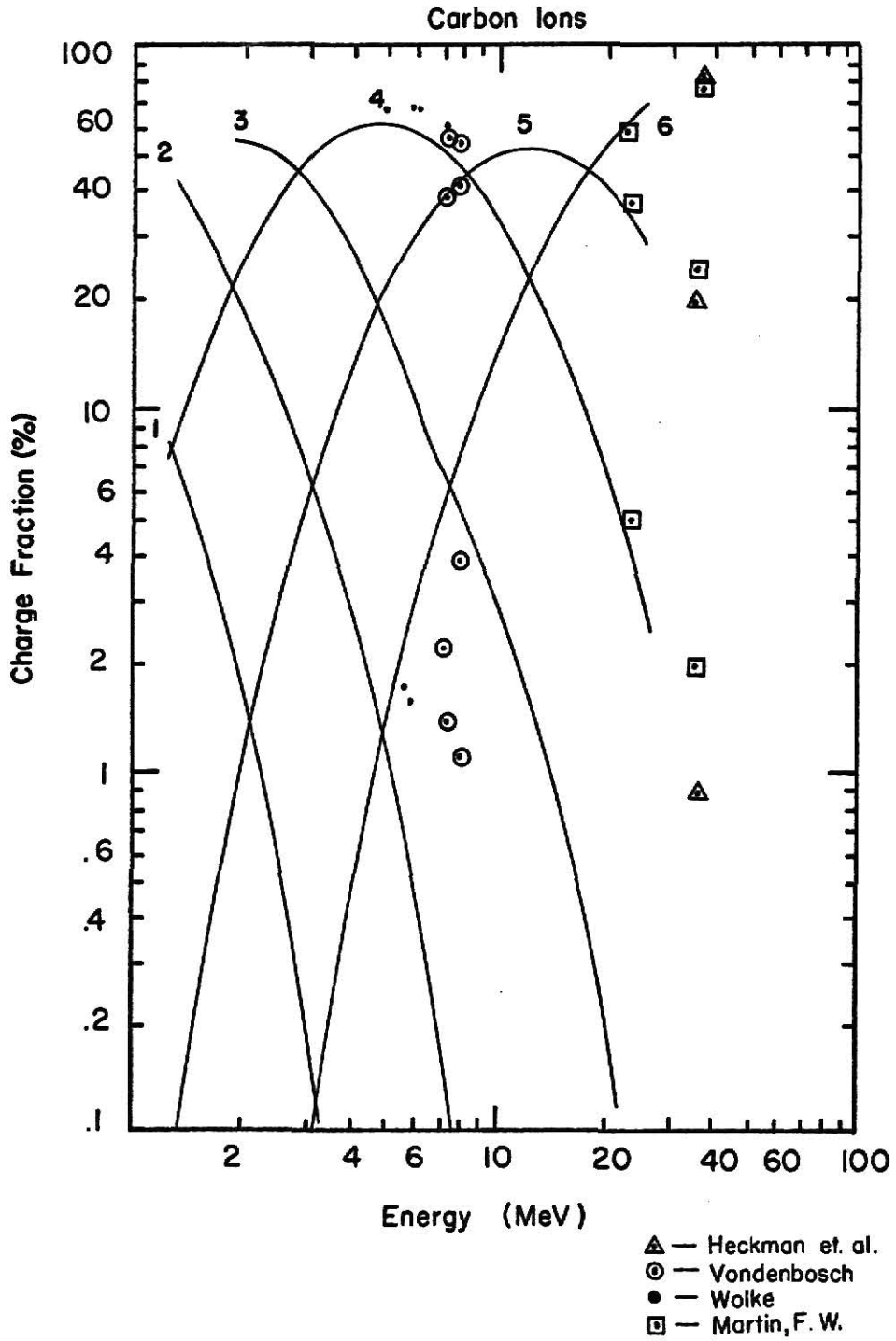
Carbon Ions
Charge Fraction (%)
Energy (MeV)
100
60
40
20
10
6
4
2
1
.6
.4
.2
.1
2
4
6
10
20
40
60
100
1
2
3
4
5
6
Heckman et. al.
Vondenbosch
Wolke
Martin, F. W.

Fig. 15

Fig. 16. Comparison of previous nitrogen data with the data of this experiment.

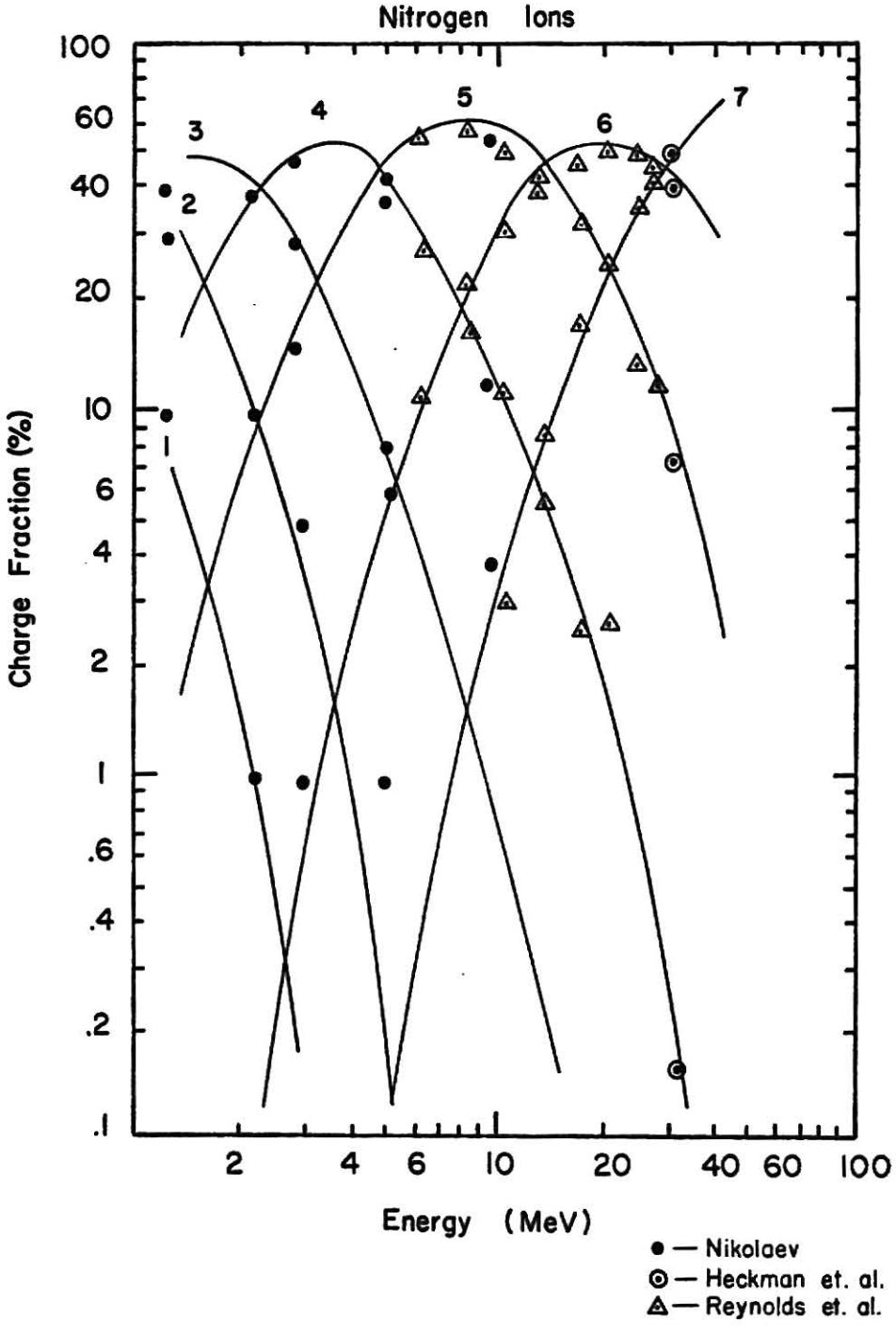
Nitrogen Ions
Charge Fraction (%)
100
60
40
20
10
6
4
2
1
.6
.4
.2
.1
1
2
3
4
5
6
7
2
4
6
10
20
40
60
100
Energy (MeV)
● — Nikolaev
⊙ — Heckman et. al.
△ — Reynolds et. al.

Fig. 16

Fig. 17. Comparison of previous fluorine data with the experimental data of this experiment.

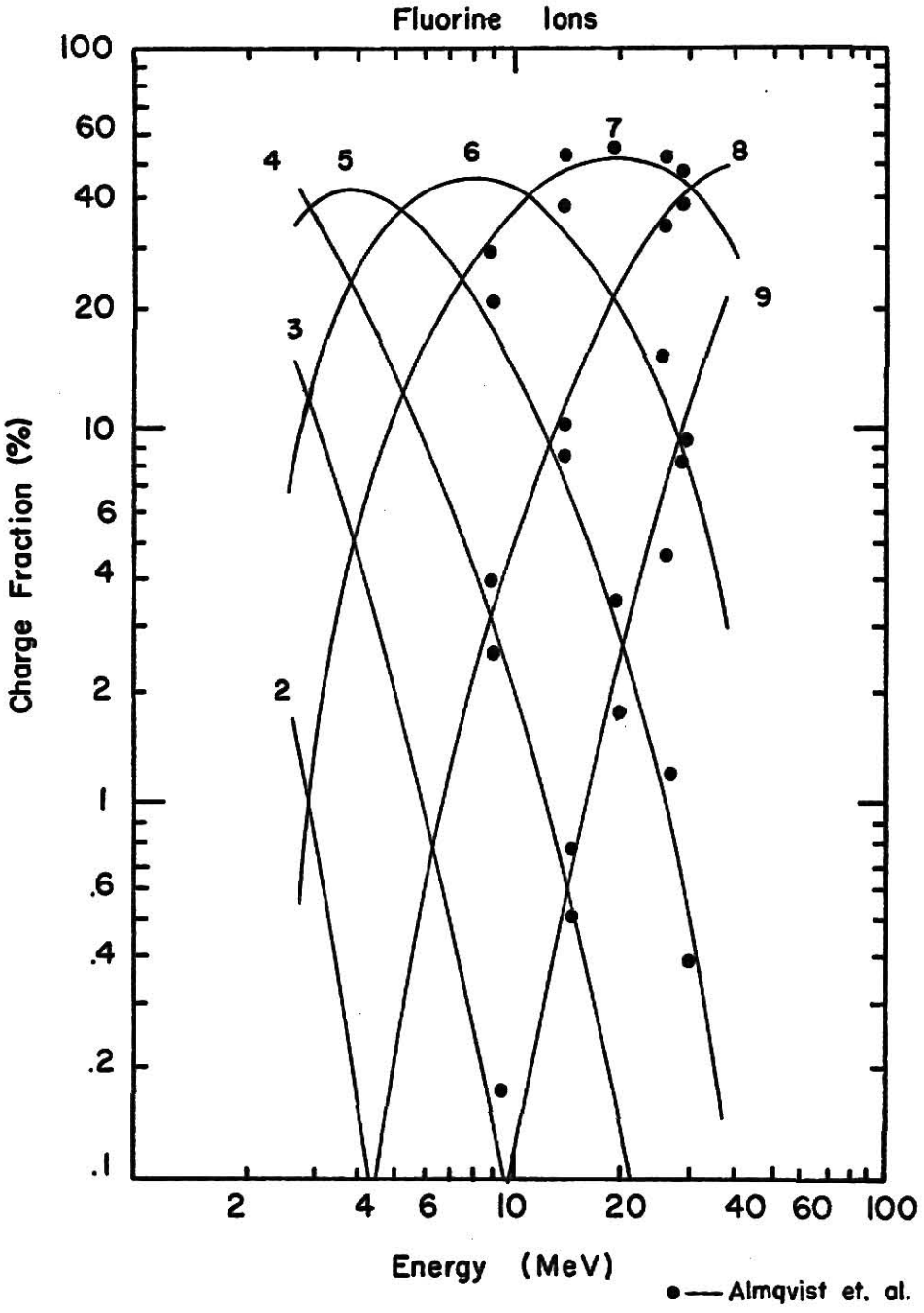
Fluorine Ions
Charge Fraction (%)
100
60
40
20
10
6
4
2
1
.6
.4
.2
.1
2
3
4
5
6
7
8
9
2
4
6
10
20
40
60
100
Energy (MeV)
●— Almqvist et. al.

Fig. 17

Table I: Non-equilibrium Distributions Data for $^{19}F \rightarrow C$ in 10 $\mu g/cm^2$ foils.

Incident Charge State	Charge Fractions (%)				
			51 MeV		
	9+	8+	7+	6+	5+
9+	49.48	40.52	9.46	0.53	0.016
7+	25.32	50.40	22.85	1.38	0.04
6+	22.73	49.55	26.12	1.58	0.023
			54 MeV		
9+	52.65	38.95	7.99	0.39	0.008
6+	25.25	51.46	21.77	1.48	0.034

The varying incident charge states are given in the vertical column and the emergent charge fractions of the non-equilibrium distributions are given in the horizontal columns.

IV. DISCUSSION AND CONCLUSION

A. Experimental Errors

The data was obtained by two different methods so that the analysis and error in each case was treated differently. The equilibrium distributions calculated from the charge spectra from the position sensitive detector contained error due to resolution inaccuries and normalization of two different spectra. The resolution of two different spectra is shown in Figs. 18 and 19. In one case the peak to valley ratio of the dominant charge states are approximately 8:1 whereas in the other spectrum it is approximately 4:1. In calculating the distribution it was assumed that the number of counts which overlapped between two peaks were equal. This is only approximately true but an upper limit of the possible error due to this assumption can be obtained. If the slope of a peak is extrapolated to zero with a straight line on the same semi-logarithmic plots (Figs. 18 and 19) then the number of counts in each triangle can be counted. The number of counts in each triangle were compared to the total number of counts in the peak. In spectrum I (Fig. 18) the number of counts in the overlap area is about 1.2% whereas in spectrum II (Fig.19) it is approximately 10%. These precentages represent the extreme upper limit of error because in actuality each peak contains counts from its neighboring peak so that the actual error involved is less than 10%.

Unfortunately the experimental setup did not allow an accurate simultaneous measurement of all charge states present so that normalization had to be used in order to include the lower or higher charge fractions. The normalization was done by taking the ratio of the total number of counts in the most dominant charge states resulting from a best division between charge states to be the same for both upper and lower spectra. The ratio of the numof counts in higher and lower charge states to the dominant charge states were determined and equilibrium charge fractions were computed by normalizing the sum of all states to unity.

Fig. 18. Extrapolation of chlorine spectrum data. The shaded area is about 1.2% of the total number of counts under the peak.

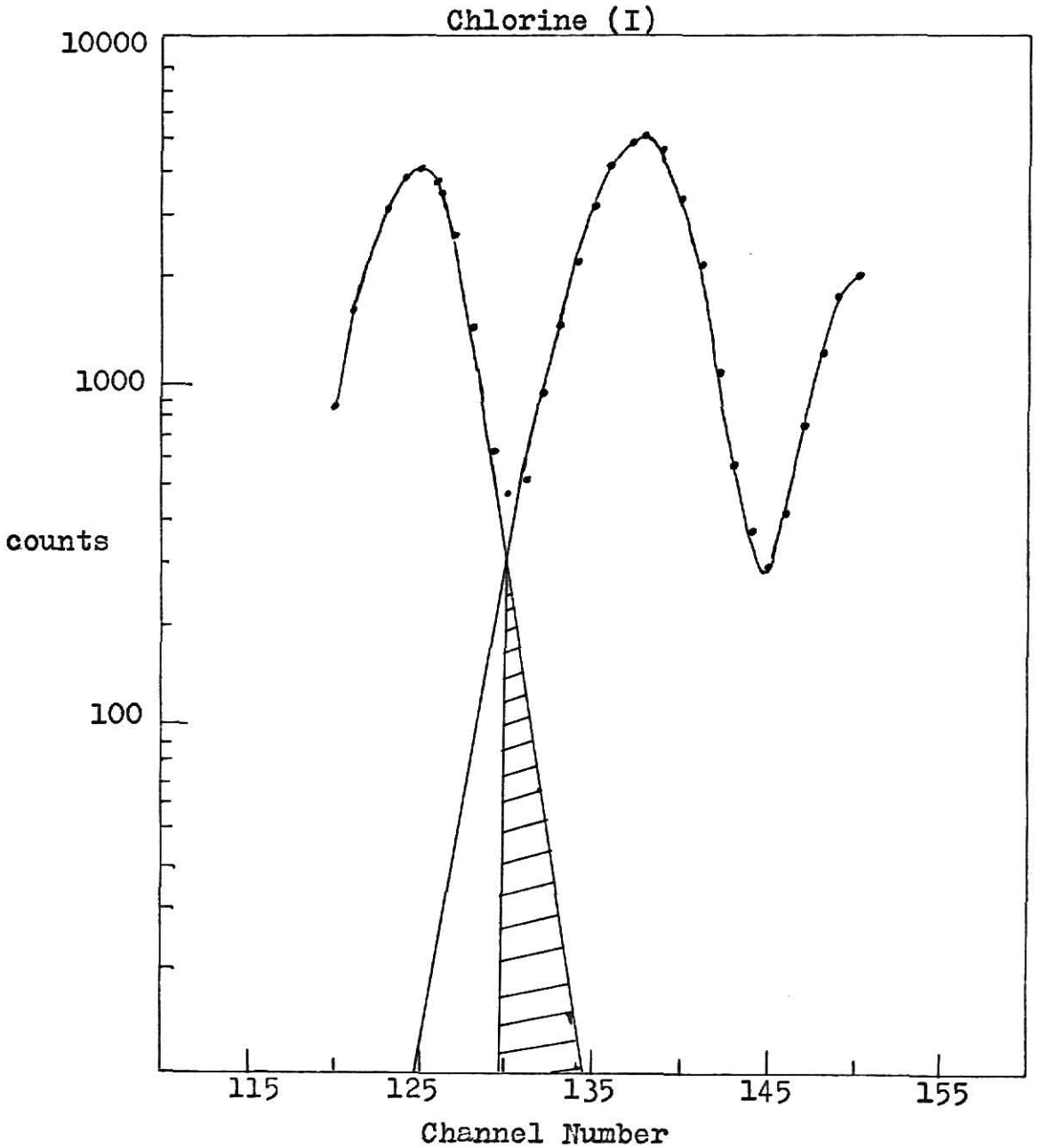
Chlorine (I)
10000
1000
100
counts
115
125
135
145
155
Channel Number

Fig. 18

Fig. 19. An extraploation of a chlorine spectrum with worse resolution. The shaded area is about 10% of the total number of counts under the peak.

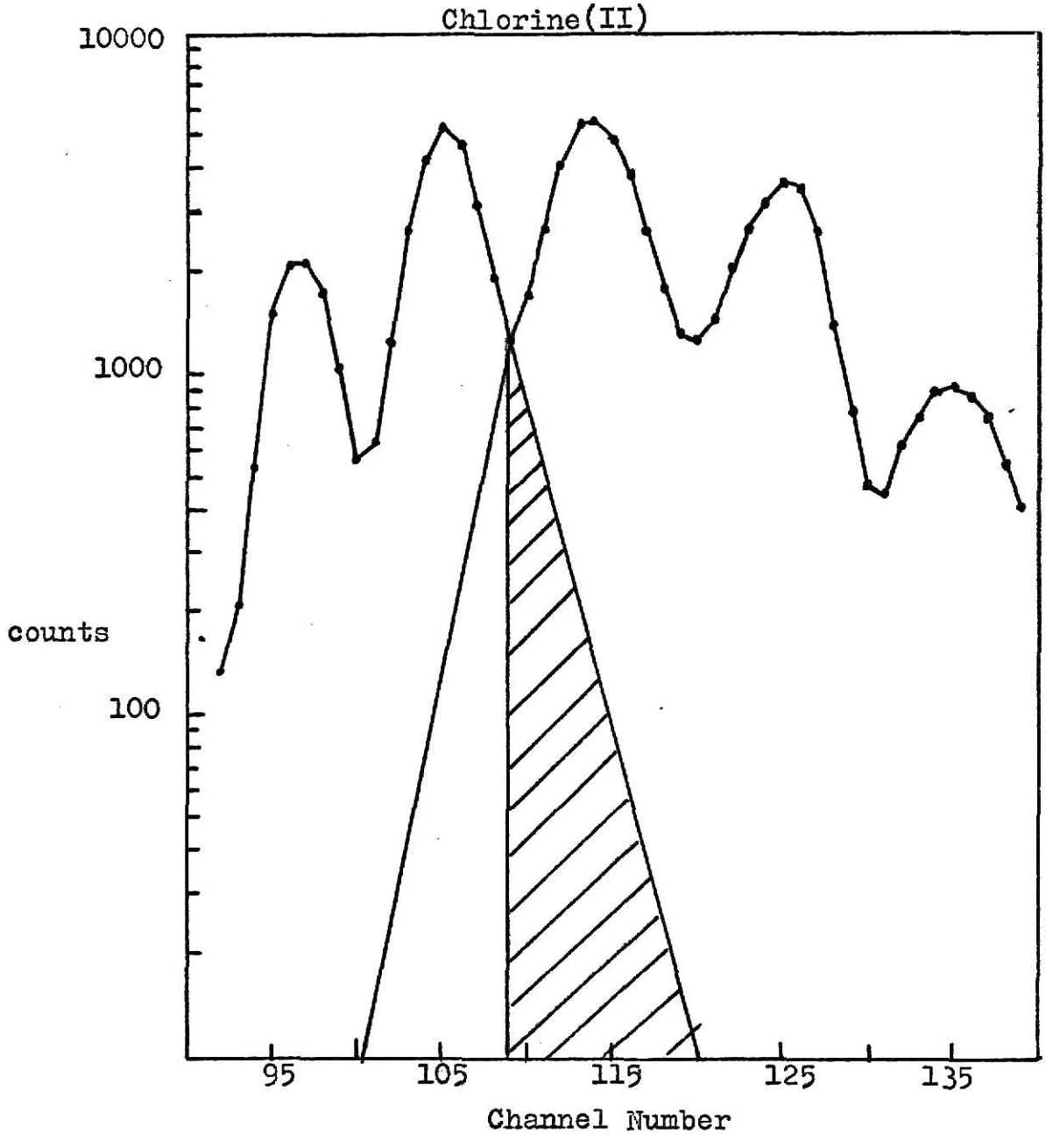
Chlorine(II)
10000
1000
100
counts
95
105
115
125
135
Channel Number

Fig. 19

The equilibrium distributions calculated from the measurements of the current of each charge state in the Faraday cup have errors mainly due to possible variations of the beam current while the measurement was being made. The problems of resolution which the spectrum data had were not present in these measurements because the charge states were all well separated.

If there was a variation in the beam current during the measurement then the calculated distribution would not be the same as the actual distribution. If the variation was rapid it could be seen on the picoammeter while the measurement was being made and such results were discarded. However a slow variation of up to 10% would not have been immediately observed. There was no way to moniter the beam current continuously but the total beam current was measured before and after the charge states were scanned. If these measurements differed by 10% or more stable operating conditions were reestablished and the measurements repeated.

The distribution calculations could have been in error because of the charge (and hence energy) purity of the analyzed beam. If the incident beam contained a non-neglibile fraction of other charge states accelerated to a different energy but the same magnetic rigidity then the various charges would be mixed in the charge analysis and the calculated distributions would not be correct. This condition was highly dependent upon the focusing condition of the accelerator and care was taken to ensure that no contaminant beams were present with an intensity greater than 0.1%.

The energy of the incident ion was determined by the field of the analyzing magnet to within an accuracy of $\pm$ 10 keV. The emergent energy of the ion was determined using the energy loss calculation of Northcliffe (15) and an estimate of the thickness of the carbon foils accurate to about 10% was made. The stopping power data is accurate to approximately 10% so that the error in the energy loss is about 15%. Because the calculated

energy loss varied from about 100 keV for the lighter ions at higher energy to about 500 keV for chlorine ions at low energy, the error in the energy of the emerging ions ranged from about 20 keV to 80 keV. The determination of the equilibrium charge fractions are uncertain by amounts ranging from about 10% for the dominant charge states to perhaps a factor of 2 for the states less than 1%. The combined error of the energy determination and the charge fraction measurements give the data presented in this thesis an accuracy of no greater than 20%. The reproducibility of the data as shown by the scatter in the points in Figs. 11, 12, 13, and 14 is comparable with this estimate.

The agreement of the present measurements with various earlier experiments is shown in Figs. 15, 16 and 17.

B. Proof of Equilibrium

In order to determine whether or not equilibrium has been reached two criteria that have been discussed previously were used. The first criteria was that the distribution remain unchanged when the incident charge state is changed at the same energy. Table II shows a distribution for chlorine ions at 30 MeV where the incident charge state was changed. There is no significant difference between the two distributions, the slight variations are well within experimental error and the conclusion is made that the distribution is representative of equilibrium.

The second criterion was that changing the foil thickness does not change the distribution. This was done and the results are shown in Table III for chlorine ions at 30 MeV in 10 and 20 $\mu g/cm^2$ foils. The distributions are again within experimental error with the exception of the high and low charge states. As was said before varying the thickness of the foil will cause the ion to loose different amounts of energy so that only if the variation inthickness is not too great will the distribution remain the same if equilibrium has been reached. In this case

Table II. Equilibrium charge distributions of 30 MeV ions for incident charge states 6+ and 7+.

Incident charge state	Charge Fractions								
	6+	7+	8+	9+	10+	11+	12+	13+	14+
6+	0.01	0.17	1.85	9.42	25.1	34.3	22.1	6.13	0.98
7+	0.02	0.19	1.90	10.0	26.2	32.8	22.2	6.14	0.72

Table III. Equilibrium charge distributions of 30 MeV chlorine ions in 10$\mu g/cm^2$ and 20$\mu g/cm^2$ carbon foils.

Foil thickness ($\mu g/cm^2$)	Charge Fractions								
	6	7	8	9	10	11	12	13	14
10	0.01	0.17	1.85	9.42	25.1	34.3	22.1	6.13	0.98
20	0.09	0.10	1.68	10.0	25.0	34.5	20.9	6.22	1.58

the variation of foil thickness does not appreciably change the dominant charge fractions but the non-dominant charge ones are drastically affected. It is apparent that the 20 $\mu g/cm^2$ foil produces more error in both the highest and lowest states.

These same tests were done at other energies and equilibrium was reached except at the highest energy data points. It can be seen from Table I that at 51 MeV and 54 MeV some charge fractions changed by as much as 50% when the incident charge state was changed so that equilibrium was not reached.

C. Cross Section Ratios

The ratio of equilibrium charge fractions (F_i/F_{i+1}) have been plotted against the velocity of the ion (Figs. 20 and 21). These points have been compared to a plot of the ratio of the loss to capture cross sections as given in eq. 36. Figure 20 shows the comparison with the charge fraction ratios for charge states 10 and 11 of chlorine. In this case the outer electrons are in the L-shell (the M-shell is fully stripped) and binding energies for these electrons can be used to determine electron velocities to be used in eq. 37. The smooth curve comes from the theoretical prediction and the crosses denote the experimental ratios. The agreement is excellent throughout the velocity range. In the case of equilibrium charge fraction ratios of electrons in the M-shell of chlorine (Fig. 21) the charge fraction ratios of charge states 4 and 5 are compared with the theoretical estimates of the cross sections for loss and capture (smooth curve). The agreement is poor in this case. The velocity dependence is too low hence the capture cross section is lower than estimated by theory. This possiblely could be due to the effect of Auger processes which will cause the loss cross sections to increase.

D. Average Charge

The mean ionization was calculated from the experimental data using the formula

Fig. 20. A plot of the ratio of the loss to capture cross sections for charge states 10 and 11 against the velocity of the ion. The solid line represents the theoretical curve given by eq. 36 and the crosses represent the experimental data points. $v_e = 1.3(10^9)$ cm/sec. .

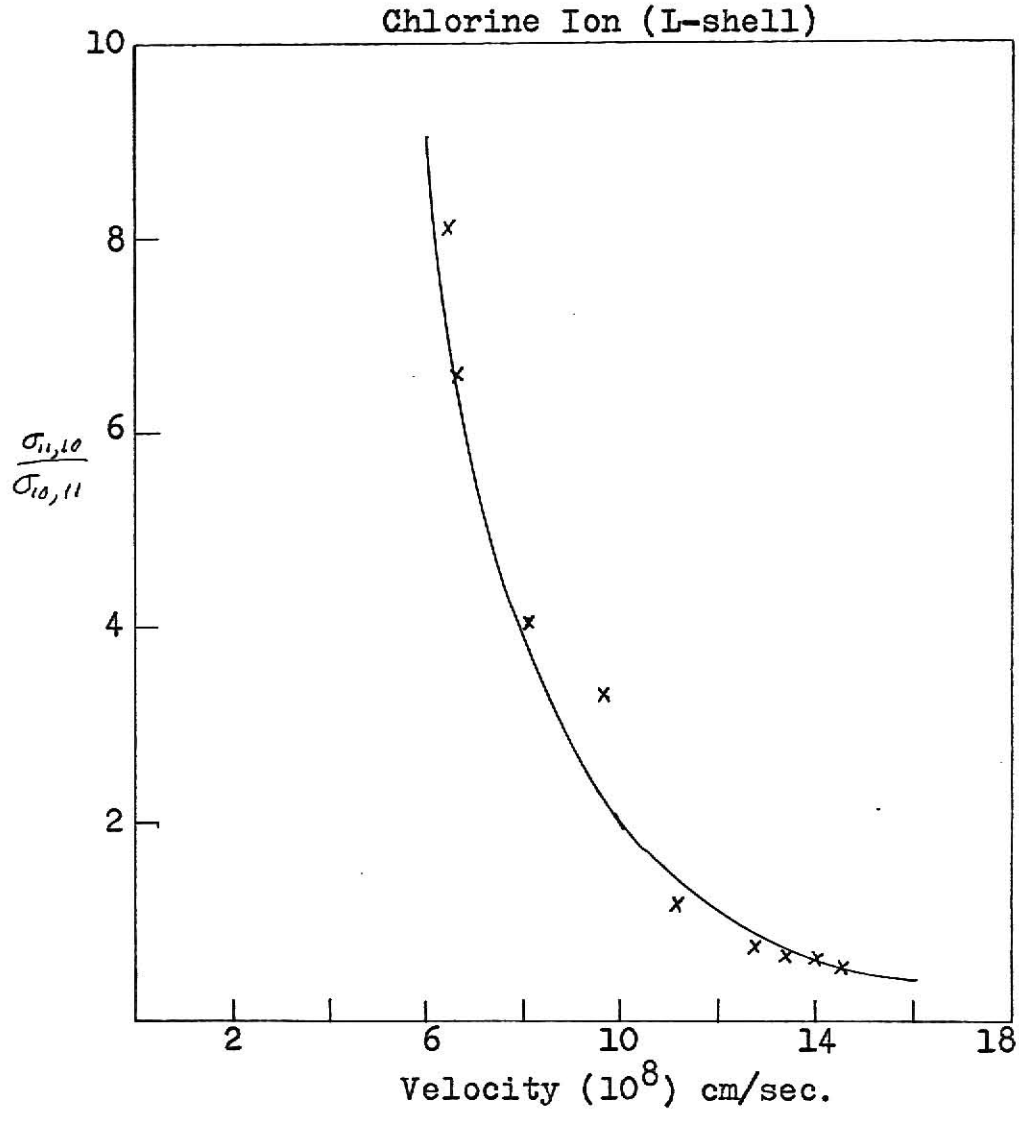
Chlorine Ion (L-shell)
10
8
6
4
2
$\frac{\sigma_{11,10}}{\sigma_{10,11}}$
2
6
10
14
18
Velocity (10^8) cm/sec.

Fig. 20

Fig. 21. A plot of the ratio of the loss to capture cross sections for charge states 4 and 5 (solid line) against the velocity of the ion. The ratio of the charge charge fractions for the same charge states are represented by x. $v_e = 4.2(10^8)$cm/sec. .

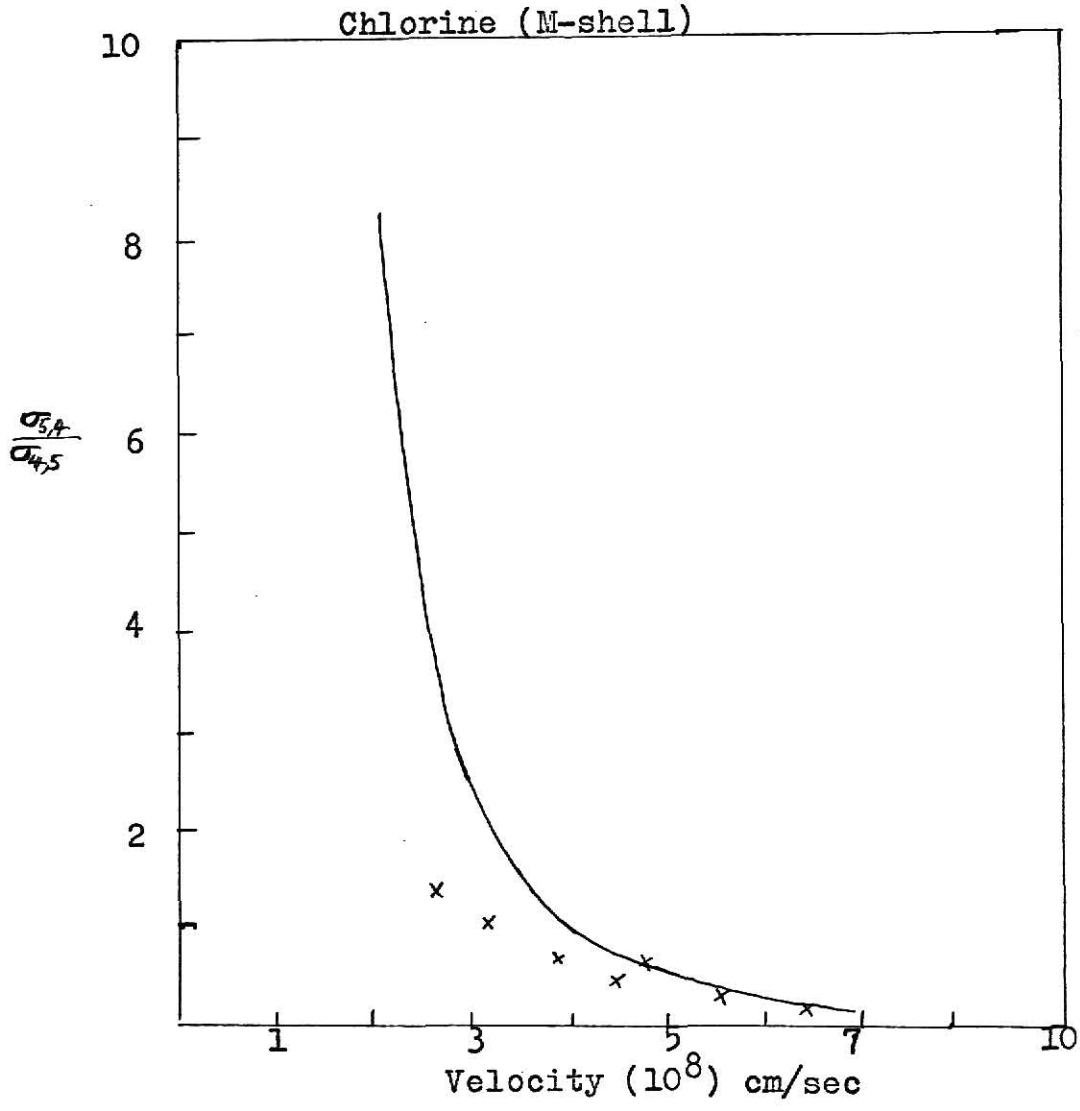
Chlorine (M-shell)
10
8
6
4
2
$\frac{\sigma_{5,4}}{\sigma_{4,5}}$
1
3
5
7
10
Velocity (10^8) cm/sec

Fig. 21

$$\bar{i}/Z = \sum_i iF_i/Z \qquad (40)$$

Using Bohr's estimate as given in eq. 38 a comparison between the experimental data and the theoretical estimate is useful. A plot of the mean ionization against the velocity is shown in Fig. 22 for both experimental points and the theoretical estimates of eq. 38. At lower velocities the data points are within 20% but as the velocity of the ion increases the agreement is not as good. This is not surprising because the statistical model gives a poor description of the velocity distribution of the inner shell electrons. It is clearly evident that Bohr's model is less than adequate for lower atomic mumber ions (Fig.23).

Brunnings, Knipp and Teller (17) have used a scaling factor which gives a somewhat better fit to the experimental data. The scaling has more of an emperical basis than theorectical.

The mean charge of fluorine ions in a gas and a solid has been compared in Table IV. The equilibrium charge fractions for the fluorine ion in a gas have been calculated from the measured cross sections for charge exchange (19). It can be seen from the data that there is a 5-20% difference between the mean charge of a heavy ion in a gas and a solid. The difference in the mean charge is in rough agreement with the estimates given by Nikolaev (8).

Bohr and Lindhard (6) have attributed the higher degree of ionization in a solid to the shorter time between collisions in solids (6).

Fig. 22. A plot of the mean ionization of fluorine against the velocity of the ion. • represents the experimental points, Δ represents Brunnings et. al. theoretical points and x represents the theoretical points of Bohr.

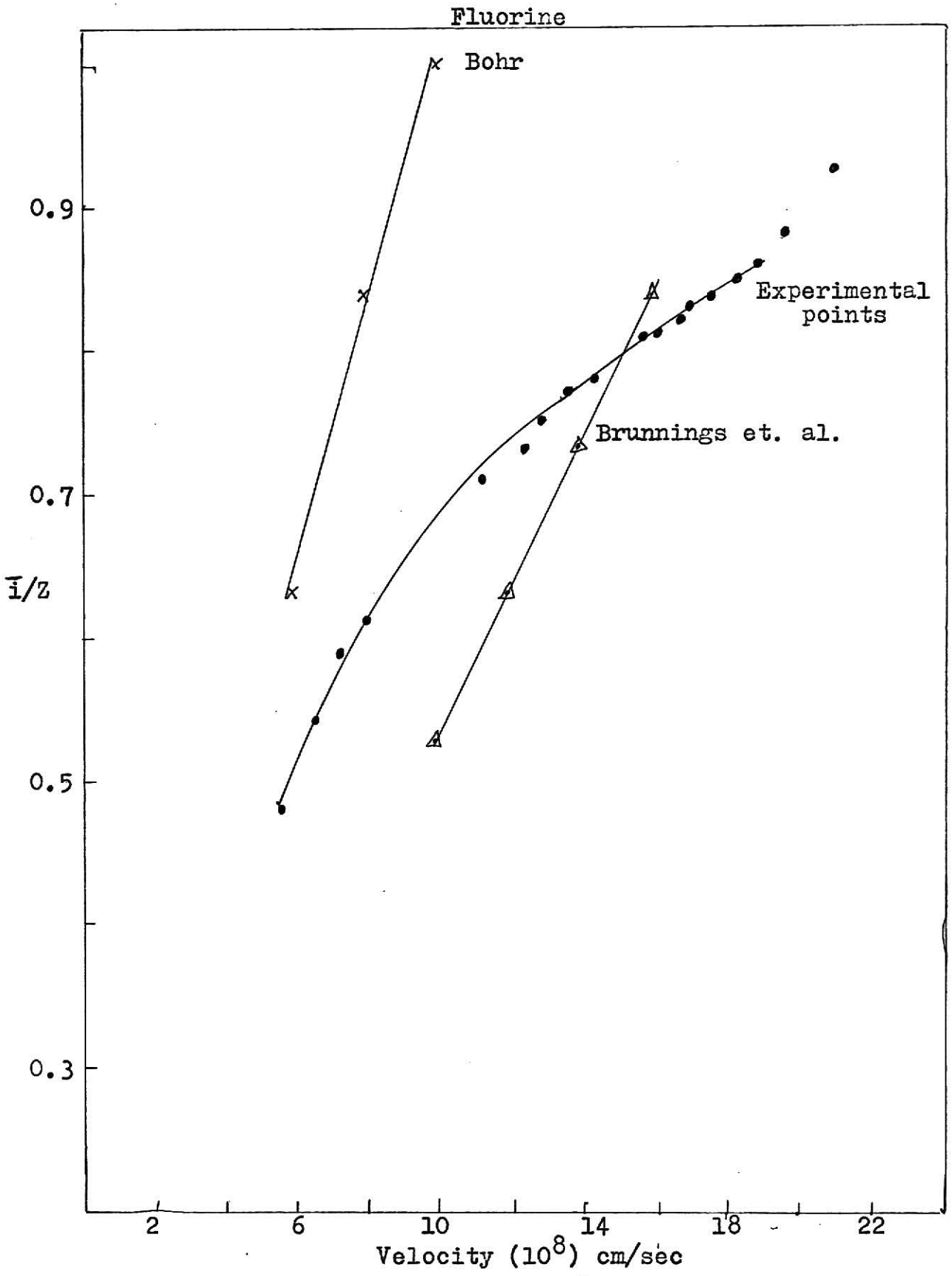
Fluorine
Bohr
Experimental points
Brunnings et. al.
0.9
0.7
0.5
0.3
$\bar{i}/Z$
2
6
10
14
18
22
Velocity (10^8) cm/sec

Fig. 22

Fig. 23. A plot of the mean ionization of chlorine ions against the velocity of the ion. x represents the theoretical points of Bohr and • represents the experimental points from this experiment.

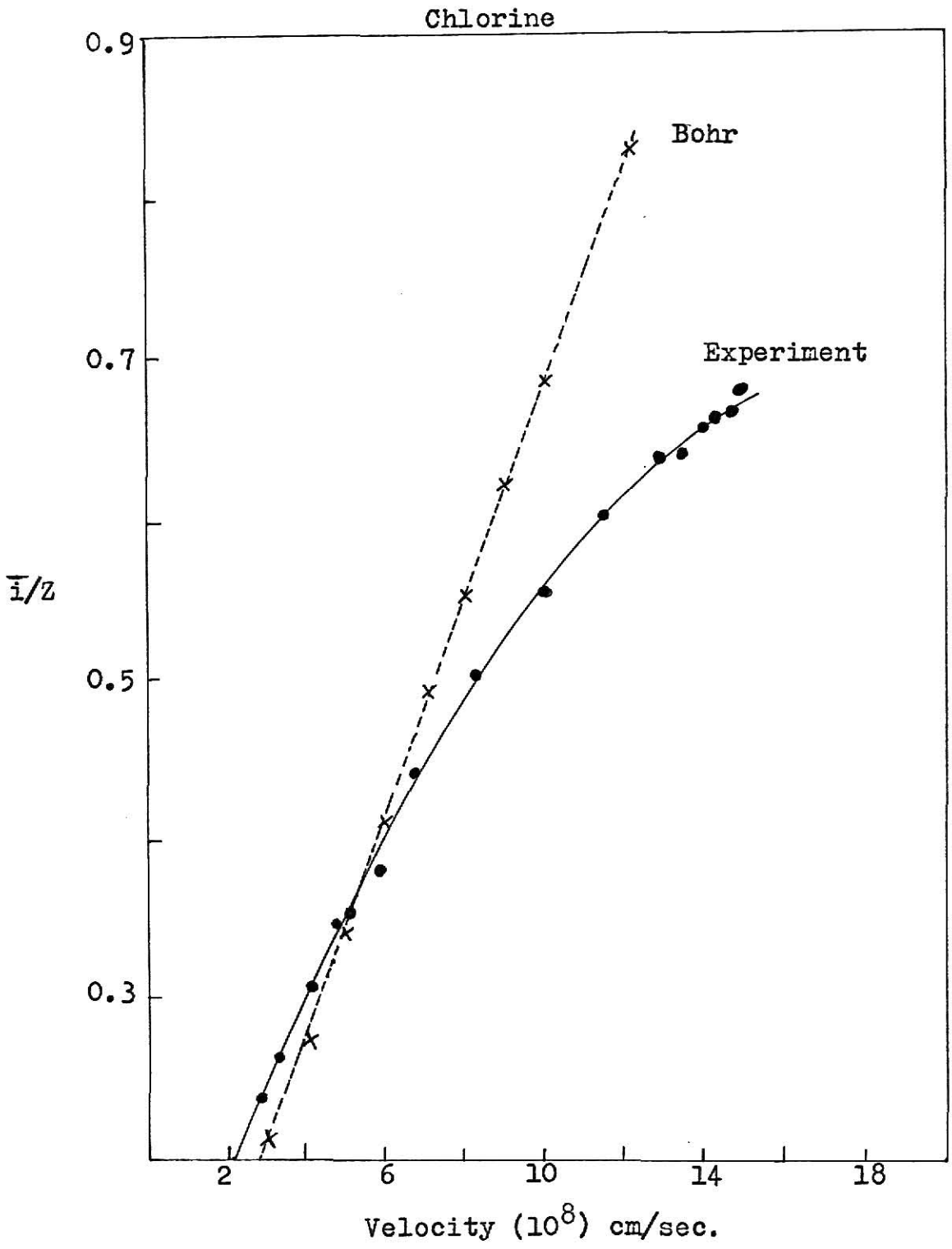
Chlorine
0.9
0.7
0.5
0.3
$\bar{i}/Z$
Bohr
Experiment
2
6
10
14
18
Velocity (10^8) cm/sec.

Fig. 23

Table IV. Mean charge of fluorine ions in argon and carbon foils.

Energy(MeV)	$\bar{i}$(argon)	$\bar{i}$(solid)	%difference
5.0	4.03	5.3	20
17.5	6.4	6.9	7
19.5	6.6	7.0	6

E. Conclusion

Equilibrium distributions were measured for chlorine, fluorine nitrogen and carbon ions from 1 MeV to 48 MeV in carbon foils with thickness from 10-20 $\mu g/cm^2$. Experimentally the criteria for equilibrium were tested to insure that the distributions obtained represented equilibrium conditions. The data of this experiment were found to be in general agreement with previous data.

Non-equilibrium distributions were measured at 51 MeV and 54 MeV in 10 $\mu g/cm^2$ foils. From this data it was determined that a target thickness of less than 10^{18} atoms/cm^2 produced equilibrium distributions of chlorine ions at 48 MeV. However at higher energies thicker targets would be necessary.

In an attempt to relate the data obtained to some theoretical estimates a comparison was made between the mean ionization data obtained in this experiment and the estimate of eq. 38 derived by Bohr. At lower velocities the experimental and theoretical values differ by less than 20%. However the agreement was not as good at higher velocities where the theoretical prediction overestimates the mean ionization by more than a factor of two. This discrepency is attributed to inadequacies of the statistical model for the inner shell electrons involved in charge transfer at high energy.

From the charge fraction data for chlorine ions, ratios of capture and loss cross sections were derived for electrons that could be identified with particular atomic shells. This data was compared to the theoretical estimate of σ_c/σ_l derived by Bohr and Lindhard (6) for both Land M shell electrons. The theoretical prediction accurately describes the velocity dependence of σ_c/σ_l(L) but fails for the more loosely bound electrons. The influence of the Auger process that is ignored in the theoretical model would account for the small value of σ_c/σ_l(M) that was observed.

References

(1) H. Goldstein, Classical Mechanics (Addison Wesley Publishing Co., 1965)

(2) J. Lindhard, V. Nielsen and M. Schaff, Notes on Atomic Collisions I, unpublished

(3) N. Bohr, Danske Videnshab. Selsk. Mat.-Fys. Medd. 18, no. 8 (1948)

(4) E. Everhart, G. Stone, and R. J. Carbone, Phys. Rev., 99, 1287 (1955)

(5) J. D. Jackson, Classical Electrodynamics (John Wiley & Sons, Inc., 1967)

(6) N. Bohr and J. Lindhard, Dan. Mat. Fys. Medd. 28, no. 7 (1954)

(7) G. I. Bell, Phys. Rev., 90, 4, 549

(8) V. S. Nikolaev, Soviet Phys. USPEKHI 8, 2, 269

(9) Almqvist, Broude, Clark, Kucher and Litherland, Can. J. Phys. 40, 954 (1962)

(10) R. L. Wolke and V. J. Sodd, Ionic and Collisional Processes

(11) F. W. Martin, Phys. Rev., 140, 1A, A75 (1965)

(12) E. Preekschat and R. Vandenbosch, Nuc. Inst. and Methods, 46, (1967)

(13) H. L. Reynolds, L. D. Wyly and A. Zucher, Phys. Rev., 98, 6, 1825 (1955)

(14) H. H. Heckman, E. L. Hubbard and W. G. Simon, Phys. Rev., 129, 3, 1240 (1963)

(15) L. C. Northcliff and R. F. Schilling, Nuc. Data Tables, Sec. A, 7, 3-4 (1970)

(16) V. S. Nikolaev, L. N. Fateeva, I. S. Dmitriev, Ir. A. Teplova, Soviet Phys. JETP 5, 5, (1957)

(17) Brunnings, Knipp and Teller, Phys. Rev. 60, 657 (1941)

(18) N. Bohr, Phys. Rev. 59, 270 (1941)

(19) S. M. Ferguson (to be published)

Acknowlegements

I would like to give my heartfelt thanks to Dr. J. R. Macdonald for his continuing patience and help with this work. Also my thanks to Dr. Louis Ellsworth, Dr. S. M. Ferguson and Tang Chiao for their help in gathering the data presented in this paper.

EQUILIBRIUM CHARGE DISTRIBUTIONS OF HEAVY IONS FROM 1 MeV TO 48 MeV

by

STEVE A. SAVOY
B.S., University of Southwestern Louisiana, 1969

AN ABSTRACT OF MASTER'S THESIS

submitted in partial fulfillment of the

requirements for the degree

MASTER OF SCIENCE

Department of Physics

KANSAS STATE UNIVERSITY
Manhattan, Kansas

1971

ABSTRACT

Equilibrium charge distributions ere measured for carbon, nitrogen, fluorine and chlorine ions from 1 MeV to 48 MeV in carbon foils. Non-equilibrium distributions were measured at 51 MeV and 54 MeV for chlorine ions and an equilibrium thickness of 10^{18} atoms/cm^2 was established. The equilibrium distribution data was conpared to data of previous experiments and good agreement was generally found. The average charge has been compared to theoretical estimates of Bohr. The charge fraction ratios F_i/F_{i+1} have been compared to estimates of the ratio of the capture and loss cross sections and rough agreement was found.